Mechanics of Materials 140 (2020) 103224

Contents lists available at ScienceDirect

Mechanics of Materials

journal homepage: www.elsevier.com/locate/mechmat

On the relative accuracy of power law analyses for uniaxial low stress steady state high homologous temperature deformation

Arsath Abbasali Ayubali*, Balasivanandha Prabu Shanmugavel, K.A. Padmanabhan

Department of Mechanical Engineering, College of Engineering Guindy, Anna University, Chennai - 600025, India

ARTICLE INFO

Keywords:
Activation energy for the rate controlling process
Power law
Steady state creep rate of deformation / minimum creep rate
Steady state structural superplastic flow
Stress exponent

ABSTRACT

If the mathematical operations are correct, uniaxial low stress, steady state high homologous temperature creep and steady state structural Superplasticity phenomena can be well described by a 'power law' that relates the applied stress to the strain rate of deformation (Padmanabhan et al., 2015). Isothermal dislocation creep, which exhibits no grain size dependence, displays a linear log strain rate – log stress relationship till there is a change in the rate controlling mechanism. In contrast, during grain-size dependent, isothermal steady state structural superplastic flow, even within narrow strain rate ranges the slope changes, notwithstanding the presence of the same rate controlling mechanism. In both the phenomena the stress exponent, n, decreases with increasing temperature even for a constant rate controlling mechanism (Padmanabhan, 1973). Four analytical methods, differing in details, are based on the power law equation, viz., a procedure used by experimental scientists, its improved variant, a method in vogue in rheology and a procedure due to Padmanabhan et al., 2015. By examining experimental data pertaining to many systems, it is demonstrated that the method of rheology does not follow the tenets of Dimensional Analysis and that the scatter in the predictions is the maximum for this case. The method of experimental scientists ignores the temperature dependence of the stress exponent and this leads to significant discrepancies between the measured and predicted properties. When mathematics is correct and the relevant physical situation is taken into account, the other two methods, i.e. the improved method of the experimental scientists and that of Padmanabhan et al., 2015, lead to similar results, but the latter analysis is more accurate because of its better normalizing procedure. It is also simpler. A missing detail in the earlier paper (Padmanabhan et al., 2015), viz., estimation of the grain-size exponent of the strain rate predicted for isothermal, steady state structural superplastic flow in terms of the Buckingham Pi Theorem is also furnished here.

1. Introduction

Research on the phenomenology of creep started quite a while ago (National Standards Body, 1948). Creep response constitutes the most important design constraint for components subjected to low to medium mechanical stresses and high temperatures, e.g. as found in modern power generation units, aero-engines (Smith et al., 1965–66).

Many components, e.g. superheater, reheater tubing, power plant boilers, have long design life, sometimes more than 250,000 h. Therefore, accelerated tests to determine the residual life of parts in service have been developed. Such investigations should ensure, in principle, industrial safety by predicting the remnant life of components in service accurately (Evans and Wilshire, 1993).

Superplastic[1] forming, in contrast, is a niche production technology, used, for example, in aerospace, automotive, architectural and sports goods industries. Steady state, isotropic superplasticity is observed within a narrow strain rate – grain size - temperature domain. For efficient superplastic forming a constitutive equation that relates accurately the rate of deformation to the stress, temperature and grain size is essential (Padmanabhan et al., 2015).

For isostructural, low stress, high homologous temperature creep and steady state superplasticity experimental scientists use an equation (Garofalo, 1965; Mukherjee et al., 1969; Raj and Langdon, 1989)

$$\dot{\varepsilon} = A_1'\left(\frac{\sigma}{G}\right)^n \exp\left(-\frac{Q}{kT}\right) \tag{1}$$

* Corresponding author.
E-mail addresses: arsathabbas@gmail.com (A.A. Ayubali), sivanandha@annauniv.edu (B.P. Shanmugavel), kap@annauniv.edu (K.A. Padmanabhan).

[1] In this paper "superplasticity" refers to structural/ grain-size sensitive superplasticity. The other type, viz., environmental superplasticity, displays no grain size dependence. For that class the analysis for steady state low stress, high homologous temperature creep in the region where it is grain size independent discussed in this paper applies.

https://doi.org/10.1016/j.mechmat.2019.103224
Received 23 April 2019; Received in revised form 25 October 2019; Accepted 25 October 2019
Available online 28 October 2019

where in general A_1' and n depend on material, temperature, and grain size (which is often kept constant). This formulation is consistent with the tenets of dimensional analysis for constant n (independent of both σ and T), as σ and T are presented dimensionless. An alternative equation is also extensively used (Eqn 2), viz.

$$\dot{\varepsilon} = A_2''\left(\frac{G}{T}\right)\left(\frac{\sigma}{G}\right)^n \exp\left(-\frac{Q}{kT}\right) \tag{2}$$

Here A_2'' is another constant. This equation also is dimensionally correct for constant n, if the dimension of A_2'' is chosen appropriately.

If the structure terms are lumped into an average grain size L, Eq. (1) becomes (Eqn 1a)

$$\dot{\varepsilon} = A_1''\left(\frac{b}{L}\right)^p\left(\frac{\sigma}{G}\right)^n \exp\left(-\frac{Q}{kT}\right) \tag{1a}$$

where A_1'' and p are constants and b is the Burgers vector.

The above generic equations are assumed to describe all physical mechanisms of high temperature deformation, with different numerical values assigned to the constants for different physical mechanisms.

However, experimental results reveal that during steady state isothermal superplastic flow, n is not independent of stress/ strain rate even within a narrow range of strain rate where the same mechanism is rate controlling and that in both creep and superplasticity n is not temperature- independent (Padmanabhan et al., 2015; Padmanabhan, 1973).

For normalization of stress, in place of the shear modulus, Padmanabhan et al. (2015) have suggested the use of a carefully selected reference stress, e.g. room temperature, uniaxial tensile (or compressive) yield stress of material. This ensures complete temperature independence, which cannot be guaranteed in the method of experimental scientists because the temperature dependences of the flow stress and the shear modulus are different. Moreover, experimental determination of room temperature yield stress is considerably easier than the measurement of shear modulus at different temperatures. In case of superplasticity, the reference stress corresponds to the stress at which $n = 1$ in the normalised stress-strain rate space and the method of calculating the same is explained in (Padmanabhan, 1977; Padmanabhan et al., 2015). In addition, these authors advocate the normalization of grain size with respect to a sufficiently large value of grain size, L_0, instead of the Burgers vector, which is relevant only to dislocation mechanisms, i.e. $(\frac{L}{L_0})^p$ is used in the latter method. Consequently, as strain rate and grain size are inversely related, p will be a negative constant.

2. The analysis

2.1. The method of experimental scientists

Apart from the problems concerning the method of experimental scientists mentioned in the previous section, the way in which the value of G, the shear modulus, of a material is determined in this procedure is rather crude. The room temperature values of G of individual elements that constitute the alloy are selected and combined using the rule of mixtures to get the value for the alloy and this is followed by an ad hoc extrapolation to a temperature of choice. However, by far the best empirical method of knowing the G value of a material at any given temperature is to use the regression equations presented by Frost and Ashby (Frost and Ashby, 1982) by analysing a large volume of experimental data. Use of these regression equations is suggested as a way of improving the analysis of experimental scientists.

2.2. Possible improvements in the method of experimental scientists

As the shear modulus has a temperature dependence different from that of the applied stress, n the stress exponent, is not temperature-independent. Ignoring this fact leads to an erroneous value for the real activation energy for the rate controlling process (Padmanabhan et al., 2015). Therefore, in the rate equation the temperature dependence of n should be taken into account in addition to determining the value of shear modulus using the regression equations given by Frost and Ashby (Frost and Ashby, 1982), as discussed in the previous section. It is pertinent to note that so far no one has evaluated quantitatively the improvement in the accuracy of predictions that will result by adopting these changes.

2.3. The method of rheology

The method of rheology is discussed in Appendixes C and D of Padmanabhan et al., 2015 for high temperature creep and steady state structural superplasticity respectively. In this method the power law equation is handled without stress normalization, which makes it inconsistent with the tenets of Dimensional Analysis. But, in this method n is treated correctly as a function of stress/ strain rate and temperature. Then, Q, the real activation energy for the rate controlling process, is obtained from the apparent activation energy values determined at constant stress, Q_σ (Eqn 4) and/ or constant strain rate, $Q_{\dot{\varepsilon}}$ (Eqn 5) with the help of the following equations.

High temperature creep

When $\sigma = \sigma_1$ and $\nu = (kT/h)$,

$$-\frac{Q_{\sigma_1}}{k} = \left(\frac{\partial \ln\dot{\varepsilon}}{\partial\left(\frac{1}{T}\right)}\right) = -\frac{Q}{k} - \frac{T^2}{T_1}\left(\frac{\partial n_0}{\partial T'}\right)\ln\sigma_1 + \frac{T^2}{T_1}\left(\frac{\partial n_0}{\partial T'}\right)\ln\sigma_c \tag{3}$$

By plotting experimental $\ln\dot{\varepsilon}$ against $(1/T)$ at constant pre-selected stress, σ_1 the value of $Q_{\sigma_1}$is determined. In Eqn. (3), the temperature, T corresponds to T_{mean} $(= (T_1 + T_2)/2)$ and $T' = (T - T_1)/T_1$. In this case all values other than Q, the real activation energy, are known and this value can be obtained by the method of least squares from the apparent activation energy values determined at various constant stress levels.

When $\nu = 10^{13}s^{-1}$,

$$\frac{-Q_{\sigma_1}}{k} = T - \frac{Q}{k} - \frac{T^2}{T_1}\left(\frac{n_0}{T'}\right)\ln\sigma_1 + \ln\frac{T^2}{T_1}\left(\frac{n_0}{T'}\right)\ln\sigma_c \tag{4}$$

When $\nu = (kT/h)$, $\dot{\varepsilon} = \dot{\varepsilon}_1$ and $A_5 = (\ln\dot{\varepsilon}_1 + 1 - \ln A_3)$,

$$Q_{\dot{\varepsilon}1} = k\left(\frac{\partial \ln\sigma}{\partial\left(\frac{1}{T}\right)}\right)_{\dot{\varepsilon}=\dot{\varepsilon}_1} = \frac{Q}{n_0(T)}\left[1 + \frac{T}{T_1 n_0(T)}\frac{\partial n_0(T)}{\partial T'}\right] + A_5\frac{k}{(n_0(T))^2}.\frac{T^2}{T_1}\left(\frac{\partial n_0(T)}{\partial T'}\right) \tag{5}$$

When $\nu = 10^{13}s^{-1}$, $\dot{\varepsilon} = \dot{\varepsilon}_1$ and $A_5 = (\ln\dot{\varepsilon}_1 + 1 - \ln A_4)$, $A_4 = (10^{13}A_3.\, h/k)$

$$Q_{\dot{\varepsilon}1} = k\left(\frac{\partial In\sigma}{\partial\left(\frac{1}{T}\right)}\right)_{\dot{\varepsilon}=\dot{\varepsilon}_1} = \frac{Q}{n_0(T)}\left[1 + \frac{T}{T_1 n_0(T)}\frac{\partial n_0(T)}{\partial T'}\right] + A_5\frac{k}{(n_0(T))^2}.\frac{T^2}{T_1}\left(\frac{\partial n_0(T)}{\partial T'}\right) - \frac{kT}{n_0(T)} + \frac{kT^2\ln T}{(n_0(T))^2 T_1}\left(\frac{\partial n_0}{\partial T'}\right) \tag{6}$$

A reliable value for the real activation energy, Q can be obtained from Eqs. (3)(6). If the Q values obtained from the different equations

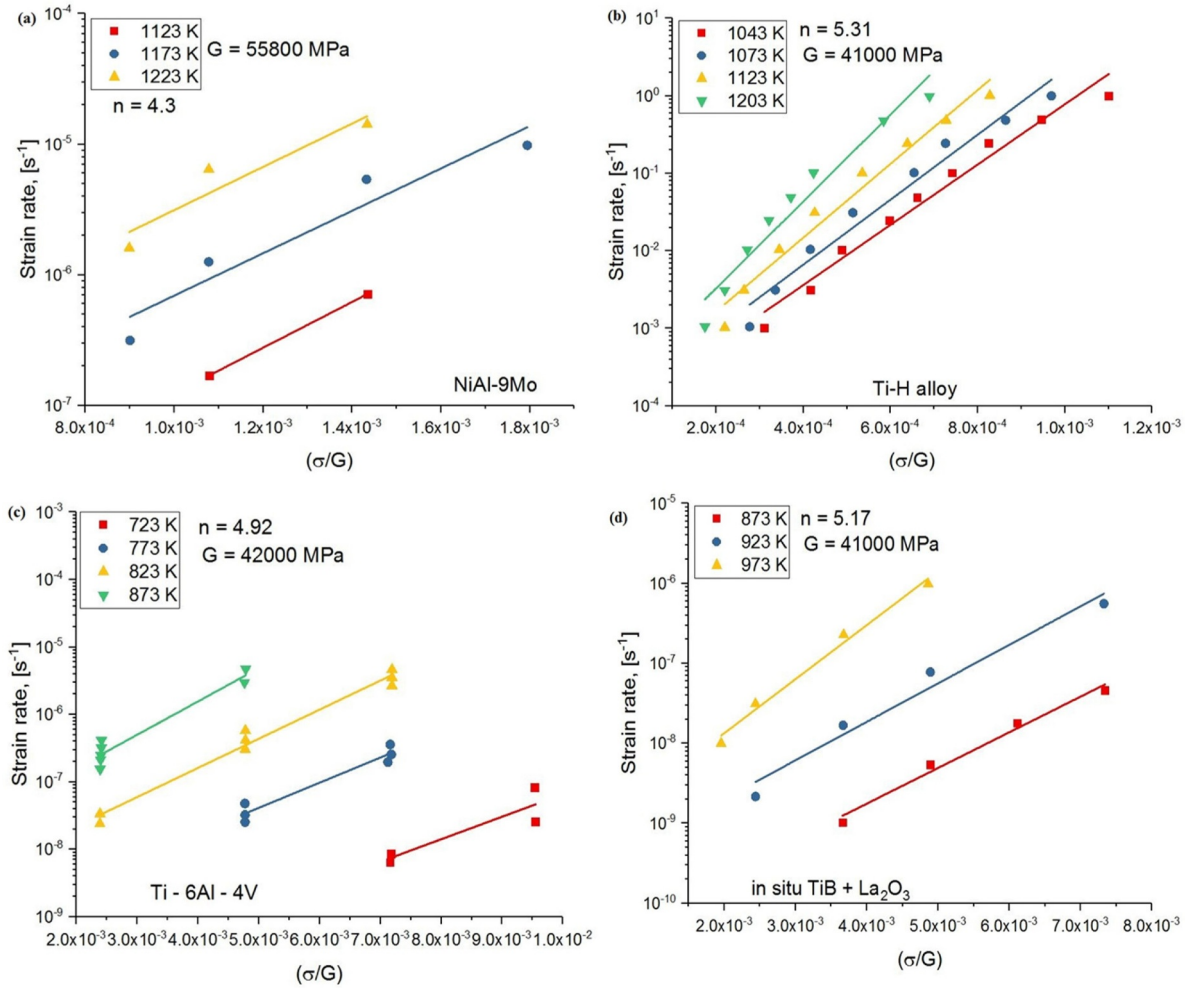

Fig. 1. Graphical representations in the method of experimental scientists where the stress is normalised with respect to the shear modulus, G of the material calculated in an approximate way (see text). Full lines are based on the equations and symbols represent the experimental points for 4 systems chosen as examples: (a) NiAl-9Mo (Weili et al., 2004), (b) Ti-H alloy (Senkov and Jonas, 1996), (c) Ti-6Al-4 V alloy (Lavinia et al., 2014), and (d) in situ TiB + La_2O_3 alloy (Lv et al., 2009).

Table 1
High temperature creep: Real activation energy for the rate controlling deformation mechanism in case of the 6 systems analysed for both $\nu = (kT/h)$ or $\nu = 10^{13}s^{-1}$ using the method of experimental scientists.

Systems	Method of Experimental scientists (mean values within parenthesis)	
	Q, [KJ/mol.] $\nu = (kT/h)$	Q, [KJ/mol.] $\nu = (10^{13}s^{-1})$
NiAl-9Mo (Weili et al., 2004) 1123 - 1223 K	346.7 – 401 (373.8)	357.1 - 411.4 (384.2)
Ti-H alloy 12at.% H (Senkov and Jonas, 1996)	146 - 209.2 (177.6)	156.4 - 218.4 (187.4)
Ti-6Al-4 V (Lavinia et al., 2014) 723 – 873K	233.4 – 319 (276.2)	243.8 - 325.77 (284.7)
TiB + La_2O_3 (Lv Xiao et al., 2009) 1123 - 1223 K	332.7 – 416 (374.3)	343.1 - 422.82 (382.9)
ZM21 Mg alloy (El Mehtedi et al., 2009) 373 - 423 K	119.4 – 170 (144.7)	129.8 - 176.31 (153.5)
2.25Cr-1.6 W Steel (Whittaker and Wilshire, 2010) 773 - 923 K	331.8 - 435.2 (383.5)	342.2 - 441.62 (391.9)

Table 2
Activation energy for the rate controlling deformation mechanism for a Ti-6Al-4 V alloy (Lavinia et al., 2014) for both $\nu = (kT/h)$ and $\nu = 10^{13}\ s^{-1}$ at different constant values of (σ/G).

Constant σ/G value	Q, $[KJ/mol.]\nu = (kT/h)$	Q, $[KJ/mol.]\nu = 10^{13}s^{-1}$
5.40E-03	318.2	323.4
5.76E-03	291.4	303.2
6.05E-03	275.9	286.4
6.37E-03	262.7	261.6
6.80E-03	241.5	256.4

given above are close, then the method can be regarded as robust.

Steady state, isotropic superplasticity

Apparent and real activation energies for steady state superplasticity

The necessary equations for determining the real activation energy for the rate controlling mechanism in case of optimal structural superplasticity are reproduced below from Appendix D of Padmanabhan et al., 2015.

When $\nu = (kT/h)$,

Table 3
High temperature creep: Computation of real activation energy calculated for both $\nu = (kT/h)$ *and* $\nu = (10)^{-13}s^{-1}$ based on an improved procedure based on the method of experimental scientists.

Systems	Improved Method of Experimental scientists (mean values within parenthesis)	
	At constant $(\frac{\sigma(T)}{G(T)})^{n(T)}$	
	Q, [KJ/mol.] $\nu = (kT/h)$	Q, [KJ/mol.] $\nu = (10^{13}s^{-1})$
NiAl-9Mo (Weili et al., 2004) 1123 - 1223 K	311.1 - 320.6 (315.8)	320.9 - 330.4 (325.6)
Ti-H alloy 12at.% H (Senkov and Jonas, 1996)	131.6 - 140.6 (136.1)	141.4 - 159.3 (150.3)
Ti-6Al-4 V (Lavinia et al., 2014) 723 – 873K	246.3 - 254.3 (250.3)	256.1 - 261.4 (258.7)
TiB + La_2O_3 (Lv Xiao et al., 2009) 1123 - 1223 K	327.4 - 337.6 (332.5)	337.2 - 344.7 (340.9)
ZM21 Mg alloy (El Mehtedi et al., 2009) 373 - 423 K	151.2 - 162.3 (156.7)	161 - 173.5 (167.2)
2.25Cr-1.6 W Steel (Whittaker and Wilshire, 2010) 773 - 923 K	294.5 - 304.2 (299.3)	304.3 - 315.9 (310.1)

$$Q_{\sigma=\sigma_1} = -k\left(\frac{\partial \ln \dot{\varepsilon}}{\partial\left(\frac{1}{T}\right)}\right)_{\sigma=\sigma_1} = \left\{Q - k\left(\frac{\partial p_0}{\partial\left(\frac{1}{T}\right)}\right)\left[1 - \ln\sigma_{ci} + \ln\sigma_1 - \frac{\sigma_1}{\sigma_{ci}}\right] - k\left(\frac{\partial \ln \sigma_c}{\partial\left(\frac{1}{T}\right)}\right)\left[p_{oi}\frac{\sigma_1}{\sigma_{ci}} - 1 - p_{oi}\right]\right\} \tag{7}$$

and

$$Q_{\dot{\varepsilon}=\dot{\varepsilon}_2} = \frac{1}{\left[1 + p_{oi} - p_{oi}\frac{\sigma_{2i}}{\sigma_{ci}}\right]}\left\{Q - k\left(\frac{\partial p_o}{\partial\left(\frac{1}{T}\right)}\right)\left[1 - \ln\sigma_{ci} + \ln\sigma_{2i} - \frac{\sigma_{2i}}{\sigma_{ci}}\right] - k\left(\frac{\partial \ln \sigma_c}{\partial\left(\frac{1}{T}\right)}\right)\left[p_{oi}\frac{\sigma_{2i}}{\sigma_{ci}} - 1 - p_{oi}\right]\right\} \tag{8}$$

In the above equations, the suffix '*i*' denotes that the value corresponds to temperature, T_i and stress, σ_{2i} corresponds to strain rate $\dot{\varepsilon}_2$ at temperature T_i. Here, p_0 is equal to $(n-1)$ as σ tends to zero in the power law stress-strain relation (Padmanabhan, 1977; Padmanabhan et al., 2015).

Table 4
Value of Q as a function of the magnitude of $(\frac{\sigma(T)}{G(T)})^{n(T)}$ that is kept constant. System NiAl-9Mo (Weili et al., 2004).

Constant $(\frac{\sigma(T)}{G(T)})^{n(T)}$ *value*		Activation Energy	
	Strainrate, $\dot{\varepsilon}$	Q, [KJ/mol.] $\nu = (kT/h)$	Q, [KJ/mol.] $\nu = (10^{13}s^{-1})$
1.18E-03	1.76E-07	320.6	330.4
1.07E-03	9.67E-07	318.2	328
5.27E-04	2.60E-06	315.5	325.3

When $\nu = 10^{13}s^{-1}$,

$$Q_{\sigma=\sigma_1} = -k\left(\frac{\partial \ln \dot{\varepsilon}}{\partial\left(\frac{1}{T}\right)}\right)_{\sigma=\sigma_1} = \left\{Q - kT_i - k\left(\frac{\partial p_o}{\partial\left(\frac{1}{T}\right)}\right)\left[1 - \ln\sigma_{ci} + \ln\sigma_i - \frac{\sigma_1}{\sigma_{ci}}\right] - k\left(\frac{\partial \ln \sigma_c}{\partial\left(\frac{1}{T}\right)}\right)\left[p_{oi}\frac{\sigma_1}{\sigma_{ci}} - 1 - p_{oi}\right]\right\} \tag{9}$$

and

$$Q_{\dot{\varepsilon}=\dot{\varepsilon}_2} = \frac{1}{\left[1 + p_{oi} - p_{oi}\frac{\sigma_{2i}}{\sigma_{ci}}\right]}\left\{Q - kT_i - k\left(\frac{\partial p_o}{\partial\left(\frac{1}{T}\right)}\right)\left[1 - \ln\sigma_{ci} + \ln\sigma_{2i} - \frac{\sigma_{2i}}{\sigma_{ci}}\right] - k\left(\frac{\partial \ln \sigma_c}{\partial\left(\frac{1}{T}\right)}\right)\left[p_{oi}\frac{\sigma_{2i}}{\sigma_{ci}} - 1 - p_{oi}\right]\right\} \tag{10}$$

In the above equations the temperature T_i stands for the mean temperature $T_{mean} = \frac{T_1 + T_2}{2}$, where T_1 and T_2 are the lower and the upper temperature limits within which the experiments are performed.

2.4. *Method of Padmanabhan et al. (2015): case of constant microstructure*

For this case the following equations are valid.

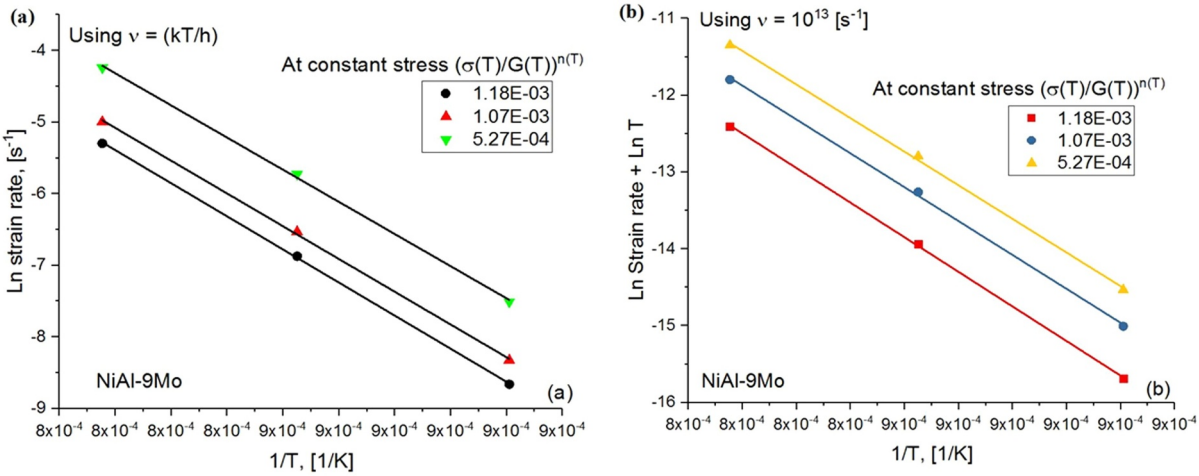

Fig. 2. (a) Plot of $ln\ \dot{\varepsilon}$ vs $(1/T)$ at constant $\left(\frac{\sigma(T)}{G(T)}^{n(T)}\right)$, (b) Plot of $(\ln\dot{\varepsilon} + \ln T)$ *vs* $(1/T)$ at constant $\left(\frac{\sigma(T)}{G(T)}\right)^{n(T)}$ for the system NiAl-9Mo (Weili et al., 2004).

Table 5
High temperature creep: Q, Q_σ and $Q_{\dot\varepsilon}$ values obtained for the 6 systems using Eqs. (3)–(6).

System	Method of Rheology					
	Q_σ, [KJ/mol.]	Q, [KJ/mol.] $\nu = (kT/h)$	Q, [KJ/mol.] $\nu = (10^{13}s^{-1})$	$Q_{\dot\varepsilon}$, [KJ/mol.]	Q, [KJ/mol.] $\nu = (kT/h)$	Q, [KJ/mol.] $\nu = (10^{13}s^{-1})$
NiAl-9Mo (Weili et al., 2004) 1123 - 1223 K	**360.1 –376.5**	**369.7–386.1**	**372.9 –397.9**	**70.2 –77.5**	**367.4 –383.7**	**375.9 –391.6**
Ti-H alloy 12at.% H (Senkov and Jonas, 1996)	**175.7 –193.9**	**195.7 –198.7**	**196.6 –203.1**	**37.2 –39.1**	**189.3 –194.5**	**195.7 –201.2**
Ti-6Al-4 V (Lavinia et al., 2014) 723 – 873K	**264.7 –277.6**	**270.9 –284.8**	**272.1 –292.5**	**60.2 –63.8**	**274.3 –286.4**	**281 –293.2**
TiB + La_2O_3 (Lv Xiao et al., 2009) 1123 - 1223 K	**370.9 –375.5**	**378.6 –383.3**	**387.9 –391.1**	**71.9 –73.1**	**380.1 –384.2**	**386.3 –389.5**
ZM21 Mg alloy (El Mehtedi et al., 2009) 373 - 423 K	**147.2 – 170.6**	**149.9 –173.4**	**168.5 –187.8**	**12.2 –15.4**	**154.2 –175.4**	**160.3 –182.1**
2.25Cr-1.6 W Steel (Whittaker and Wilshire, 2010) 773 - 923 K	**338.7 – 377.3**	**335.7 – 376.5**	**342.9 –383.0**	**44.2 –51.3**	**334.6 – 375.3**	**340.2 –381.6**

Table 6
$Q_\sigma - \sigma$, and $Q_{\dot\varepsilon} - \dot\varepsilon$ relationships and Q values for the NiAl-9Mo alloy (Weili et al., 2004) calculated using Eqs.(3)–(6).

σ [MPa]	Q_σ, [KJ/mol.]	Q, [KJ/mol.] $\nu = (kT/h)$	Q, [KJ/mol.] $\nu = (10^{13}s^{-1})$	$\dot\varepsilon$, s^{-1}	$Q_{\dot\varepsilon}$, [KJ/mol.]	Q, [KJ/mol.] $\nu = (\frac{kT}{h})$	Q, [KJ/mol.] $\nu = (10^{13}s^{-1})$
52.20	**376.5**	**386.1**	**397.9**	1.74E-06	**77.5**	**383.8**	**391.6**
58.77	**374.5**	**384.1**	**392.4**	2.62E-06	**75.2**	**380.7**	**387.6**
62.97	**370.7**	**380.3**	**386.2**	4.28E-06	**73.2**	**376.8**	**383.3**
74.28	**363.7**	**373.3**	**379.4**	5.51E-06	**72.3**	**370.1**	**378.6**
77.78	**360.1**	**369.7**	**372.9**	8.45E-06	**70.2**	**367.2**	**375.9**

Table 7
$Q_\sigma - \sigma$, and $Q_{\dot\varepsilon} - \dot\varepsilon$ relationships and Q values for the Ti-6Al-4 V alloy (Lavinia et al., 2014) calculated using Eqs.(3)–(6).

σ [MPa]	Q_σ, [KJ/mol.]	Q, [KJ/mol.] $\nu = (kT/h)$	Q, [KJ/mol.] $\nu = (10^{13}s^{-1})$	$\dot\varepsilon$, s^{-1}	$Q_{\dot\varepsilon}$, [KJ/mol.]	Q, [KJ/mol.] $\nu = (kT/h)$	Q, [KJ/mol.] $\nu = (10^{13}s^{-1})$
226.82	277.6	284.0	292.5	6.90E-08	63.8	286.4	293.2
242.10	277.6	284.8	292.3	8.82E-08	62.6	286.5	295.1
254.11	269.1	275.5	282.8	1.17E-07	61.7	279.8	287.6
267.33	264.5	271.2	279.4	1.64E-07	60.7	276.4	284
285.67	264.8	270.9	272.1	2.23E-07	60.2	274.3	281

$$\dot\varepsilon = A_3\sigma^{*n}\exp\left(-\frac{Q}{kT}\right);\ \nu = \left(\frac{kT}{h}\right), \tag{11a}$$

$$\dot\varepsilon = \left(\frac{A_4}{T}\right)\sigma^{*n}\exp\left(-\frac{Q}{kT}\right);\ \nu = 10^{13}s^{-1}, \tag{11b}$$

Here, $\sigma^* = (\frac{\sigma}{e\sigma_c})$ is the dimensionless stress, e is the base of the natural logarithms and the reference stress σ_c is greater than σ. For soundness of procedure and experimental convenience, for creep σ_c is taken as equal to the room temperature uniaxial, tensile/ compressive yield stress of the material. σ_c is the stress at which $n = 1$ in the dimensionless strain rate – stress space ($\dot\varepsilon - \sigma^*$ space) in case of superplasticity (Padmanabhan, 1977). Therefore, the condition $0 \le \sigma^* \le 1$ is always satisfied and a problem of convergence that could arise if the stress function were expanded in a power series is eliminated.

The constants A_3 and A_4 are independent of σ and T and $A_4 = (10^{13}A_3.\frac{h}{k})$. Here, h is the Planck constant and k is the Boltzmann constant.

Determination of n for low-stress uniaxial steady-state high-homologous temperature creep

From Appendix A, Eq. (A5) of Padmanabhan et al. (2015) it follows that, $n = ((\partial \ln\dot\varepsilon)/(\partial \ln\sigma)) = (1 + p) = (1 + p_0) =$ constant (n_0): $p_0 \ge 1$. Then from Eqs. 11,

$$ln\,\dot\varepsilon = ln\,C_1(T) + n_0(T)\,ln\,\sigma \tag{12}$$

From Eqn. (12), n_0 and $\ln C_1$ as functions only of temperature (as required theoretically) are obtained.

Real activation energy, Q for high temperature creep. In view of Eq. (11a) for $(\nu = (kT/h))$, $\ln\dot\varepsilon$ vs $(1/T)$ is plotted at constant $n_0(\ln\sigma - \ln\sigma_r)$ (σ_r is the reference stress which is taken to be the maximum stress employed in the experiments in the absence of knowledge about the room temperature yield stress of the industrial alloys used in the analysis). If the analysis is correct, the plot would be a straight line and the slope would equal $-Q/k$, where Q is the real activation energy for the rate controlling process, which should be independent of the magnitude of $n_0(\ln\sigma - \ln\sigma_r)$ that is kept constant. When one starts with Eq. (11b) $(\nu = 10^{13}s^{-1})$, a plot of $(\ln\dot\varepsilon + \ln T)$ *vs* $(1/T)$ at constant $n_0(\ln\sigma - \ln\sigma_r)$, again would result in a linear plot and the slope would be equal to $-Q/k$. Here also the value of Q should be independent of the magnitude of $n_0(\ln\sigma - \ln\sigma_r)$ that is kept constant.

Determination of n for steady state structural superplasticity

During steady state superplastic deformation, the stress exponent, n is strongly dependent on both stress and temperature (Padmanabhan et al., 2018). The solution, originally from Padmanabhan, 1977, is given as Eqn. (A4), Appendix A of Padmanabhan et al., 2015. For this case one obtains,

$$n = \left(\frac{\partial \ln\dot\varepsilon}{\partial \ln\sigma}\right) = (1 + p_0) - \left(\frac{p_0}{\sigma_c}\right)\sigma = B - C\sigma \tag{13}$$

Since both p_0 and σ_c are positive (Padmanabhan, 1977; Padmanabhan et al., 2015), it is predicted that n decreases linearly with increasing stress during steady state superplastic flow.

Real activation energy, Q for steady state structural superplasticity. The real activation energy for steady state superplastic flow is determined from Eqn. (8) of Padmanabhan et al., 2015, *i.e.*,

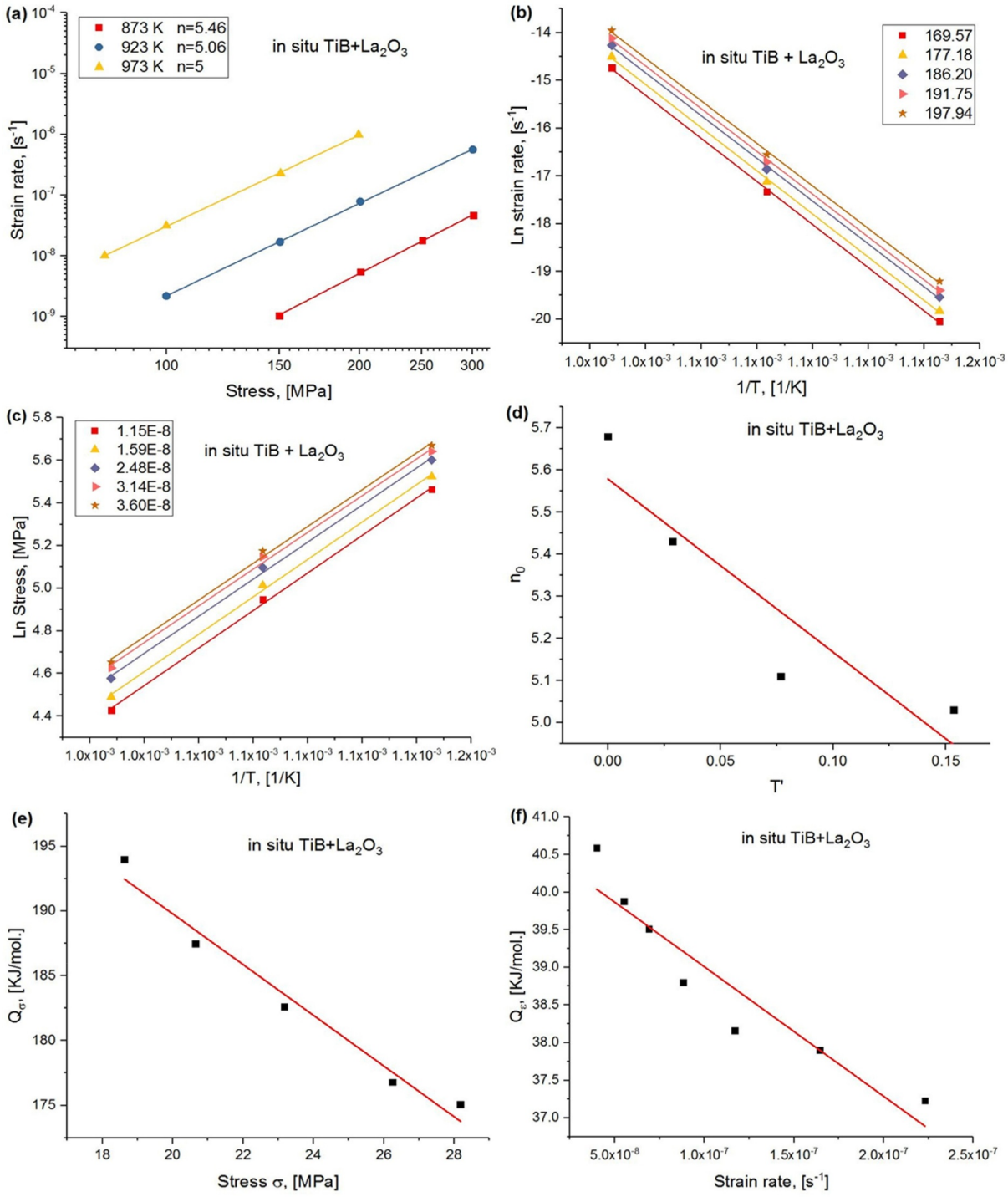

Fig. 3. (a) Double logarithmic plot of stress vs. strain rate data for in situ TiB + La_2O_3 (Lv et al., 2009), (b) $ln\ \dot{\varepsilon} - 1/T$ relation at defined constant stresses to determine the apparent activation energy Q_σ, (c) $\ln\sigma - 1/T$ relations for different constant strain rates to calculate $Q_{\dot{\varepsilon}}$, (d) n_0 as a function of T', (e) Q_σ as a function of stress from which Q is determined, and (f) $Q_{\dot{\varepsilon}}$ as a function of strain rate from which Q is determined. The values of constant stress/strain rate were chosen to cover the full range of stresses and strain rates employed in the experiments.

$$ln\,\dot{\varepsilon} = ln\,A_3 + 2p_0 + (1+p_0)\,ln(\sigma/e\sigma_c) - p_0\left(\frac{\sigma}{\sigma_c}\right) - \left(\frac{Q}{kT}\right) \tag{14}$$

or

$$(ln\,\dot{\varepsilon} + ln\,T) = ln\,A_4 + 2p_0 + (1+p_0)\,ln(\sigma/e\sigma_c) - p_0(\frac{\sigma}{\sigma_c}) - (\frac{Q}{kT}) \tag{14a}$$

The above equations correspond to the cases $\nu = (kT/h)$ and $\nu = 10^{13}s^{-1}$respectively.

When $\nu = (kT/h)$, a plot of $ln\,\dot{\varepsilon}$ vs $(1/T)$ at a constant value of $[2p_0 + (1+p_0)\ln(\sigma/(e\sigma_c)) - (p_0\,\sigma/\sigma_c)]$ is prepared, the slope of which is equal to $(-Q/k)$. The value of Q thus obtained is independent of the magnitude of $[2p_0 + (1+p_0)\ln(\frac{\sigma}{e\sigma_c}) - (p_0\frac{\sigma}{\sigma_c})]$, which is kept constant. Similarly, when $\nu = 10^{13}s^{-1}$, the slope of a plot of $(\ln\dot{\varepsilon} + \ln T)$ vs $(1/T)$ at a constant value of $[2p_0 + (1+p_0)\ln(\sigma/(e\sigma_c)) - (p_0\,\sigma/\sigma_c)]$ is equal to $(-Q/k)$. The value of Q thus obtained is independent of the magnitude of

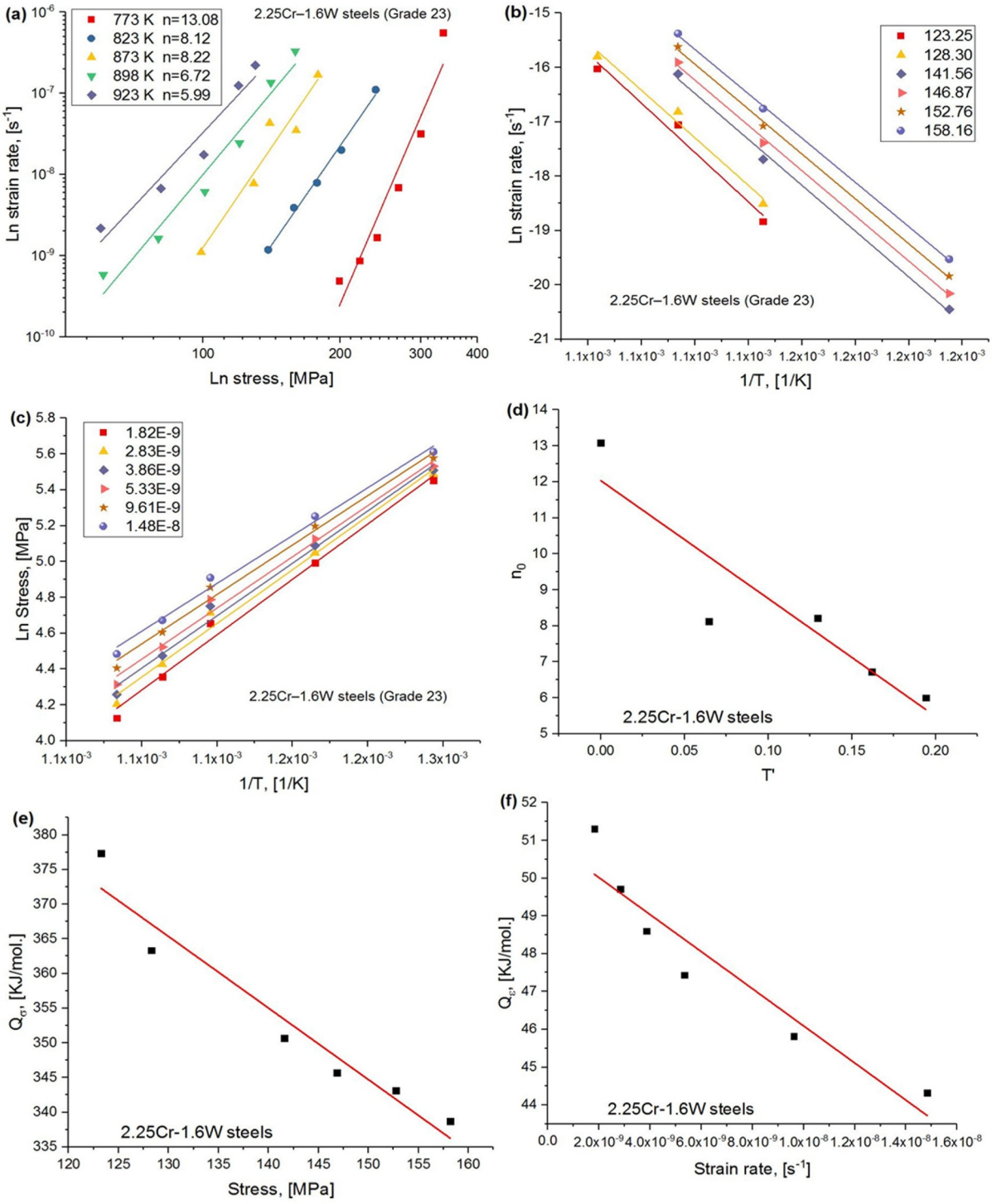

Fig. 4. (a) Double logarithmic plot of stress vs. strain rate data for 2.25Cr-1.6 W steel (Whittaker and Wilshire, 2010), (b) $ln\,\dot{\varepsilon} - 1/T$ relation at defined constant stresses to determine the apparent activation energy Q_σ, (c) $\ln\sigma - 1/T$ relation for different constant strain rates to calculate $Q_{\dot{\varepsilon}}$, (d) n_0 as a function of T', (e) Q_σ as a function of stress from which the value of Q is determined, and (f) $Q_{\dot{\varepsilon}}$ as a function of strain rate from which the value of Q is determined. The values for constant stresses/strain rates were chosen to cover the full range of stresses and strain rates employed in the experiments.

$[2p_0 + (1 + p_0)\ln(\sigma/(e\sigma_c)) - (p_0\ \sigma/\sigma_c)]$ that is kept constant.

2.5. An omission in the validation procedure adopted in Padmanabhan et al. (2015): grain size exponent for steady state superplastic flow

This missing aspect is examined here by analysing the experimental data pertaining to 4 systems.

In addition, in this paper, the method of experimental scientists, the improved procedure of experimental scientists explained above, the method of rheology and the method of Padmanabhan et al. (2015) are compared using experimental data pertaining to many systems with a view to recommending the most reliable method. An automated computer procedure has been developed. It is emphasized that when four methods are there, it is essential that one has a sound knowledge of the accuracy obtainable in each one of them. This is being done

Table 8
High temperature creep: Real activation energy for the rate controlling deformation mechanism in case of the 6 systems analysed for both $\nu = (kT/h)$ and $\nu = 10^{13}s^{-1}$.

Systems	Method of Padmanabhan et al., 2015 (mean values within parenthesis)	
	Q, [KJ/mol.] $\nu = (kT/h)$	**Q,** [KJ/mol.] $\nu = (10^{13}s^{-1})$
NiAl-9Mo (Weili et al., 2004) 1123 - 1223 K	**340.5 - 341.6** (341)	**350.3 - 351.4** (350.8)
Ti-H alloy 12at.% H (Senkov and Jonas, 1996)	**153.5 - 154.4** (153.9)	**162.8 - 163.7** (163.2)
Ti-6Al-4 V (Lavinia et al., 2014) 723 – 873K	**266.4 - 267.4** (266.9)	**272.8 - 273.8** (273.3)
TiB + La_2O_3 (Lv et al., 2009) 1123 - 1223 K	**353.7 - 354.9** (354.3)	**361.4 - 362.6** (362)
ZM21 Mg alloy (El Mehtedi et al., 2009) 373 - 423 K	**148.2 - 149.9** (149)	**166.8 - 168.5** (167.6)
2.25Cr-1.6 W Steel (Whittaker and Wilshire, 2010) 773–923 K	**337.1 - 338.7** (337.9)	**344 - 345.6** (344.8)

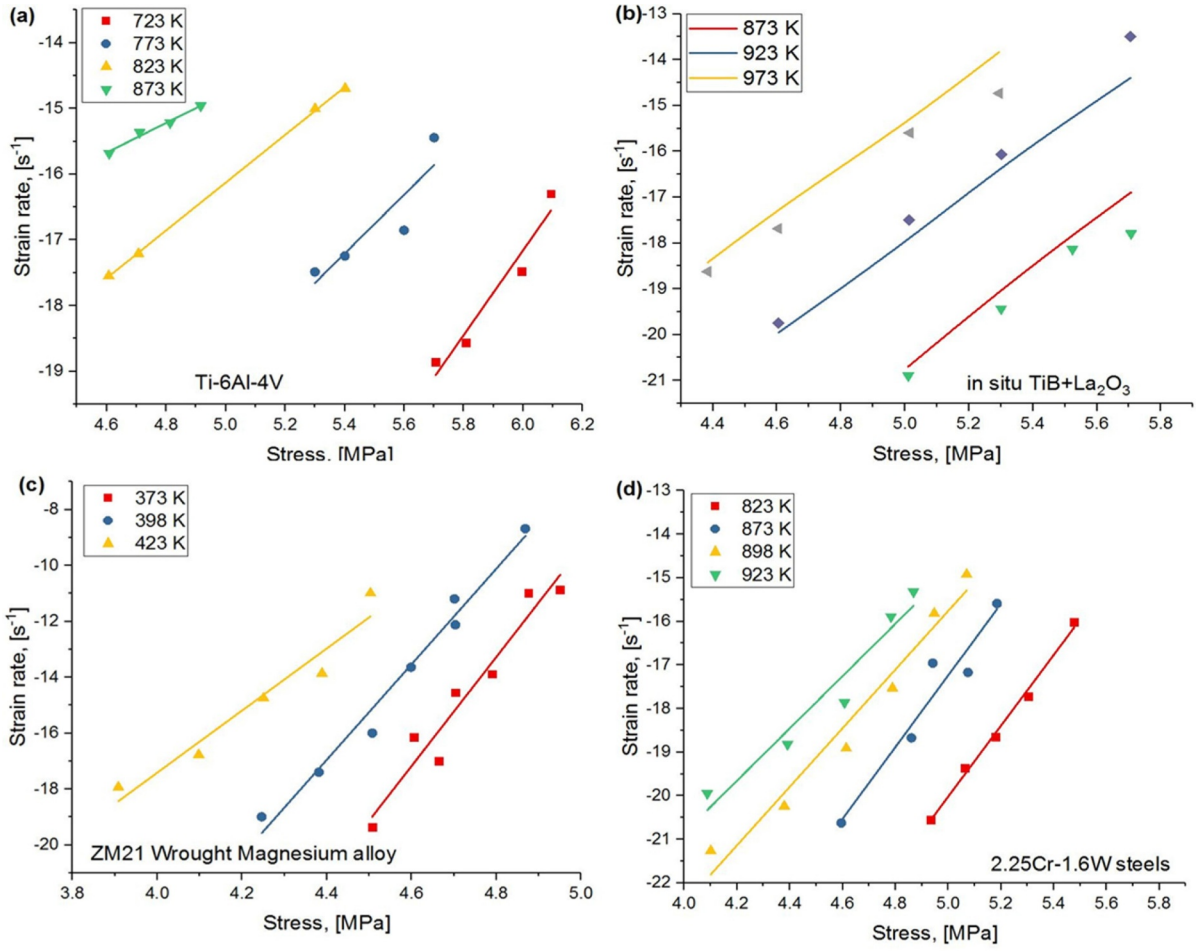

Fig. 5. Double logarithmic plot of stress vs. strain rate curves. The symbols represent the experimental points and the full lines are based on the predicted values for the four analysed systems. (a)Ti-6Al-4 V alloy (Lavinia et al., 2014), (b) in situ TiB + La_2O_3 alloy (Lv et al., 2009), (c) ZM21 Wrought Mg alloy (El Mehtedi et al., 2009), and (d) 2.25Cr-1.6 W Steels (Whittaker and Wilshire, 2010).

Table 9
Calculation for the value of Q which should be independent of the magnitude of $n_0(\ln\sigma - \ln\sigma_r)$ that is kept constant for the system Ti-H alloy 12at.% H (Senkov and Jonas, 1996).

Constant $n_0(\ln\sigma - \ln\sigma_r)$ value		Activation Energy, **Q**	
	$\ln\dot{\varepsilon}$	**Q,** [KJ/mol.] $\nu = (kT/h)$	**Q,** [KJ/mol.] $\nu = (10^{13}s^{-1})$
13.46	−6.85	154.4	161.3
12.73	−6.21	153.9	160.8
11.76	−5.46	153.6	160.6
9.51	−4.45	153.5	160.5

quantitatively for the first time in this paper.

3. Data analysis

3.1. High temperature creep

6 systems were analysed: NiAl-9Mo (Weili et al., 2004), Ti-H alloy 12at.% H (Senkov and Jonas, 1996), Ti-6Al-4 V (Lavinia et al., 2014), TiB + La_2O_3 (Lv et al., 2009), ZM21 wrought Mg alloy (El Mehtedi et al., 2009) and 2.25Cr-1.6 W Steel (Whittaker and Wilshire, 2010). The values of temperature T, stress, σ and strain rate, $\dot{\varepsilon}$ were digitized from the respective experimental plots.

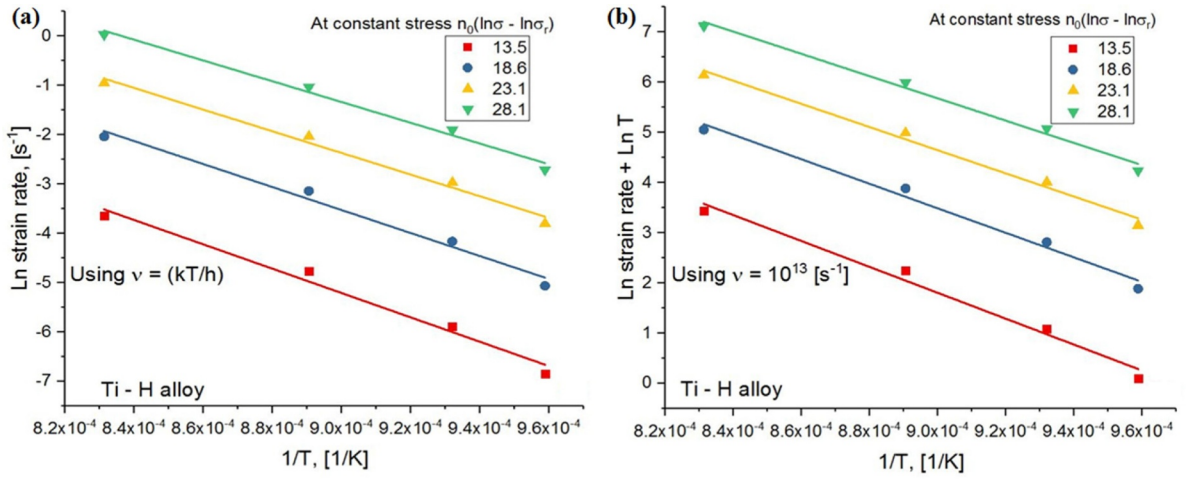

Fig. 6. (a) Plot of $ln\ \dot{\varepsilon}$ vs $(1/T)$ at constant $n_0(\ln\sigma - \ln\sigma_r)$, (b) plot of $(\ln\dot{\varepsilon} + \ln T)$ *vs* $(1/T)$ at constant $n_0(\ln\sigma - \ln\sigma_r)$, for the system Ti-H alloy 12at.% H (Senkov and Jonas, 1996).

Table 10
Comparison of the real activation energy for the rate controlling process at different constant stress levels for the different methods.

Systems	Different Constant Stress level [MPa]	Method of Experimental scientists **Q,** [KJ/mol.]	Improved Method of Experimental scientists **Q,** [KJ/mol.]	Method of Rheology **Q,** [KJ/mol.]	Method of Padmanabhan et al., 2015 **Q,** [KJ/mol.]
NiAl-9Mo (Weili et al., 2004) 1123 - 1223 K	52.20	401	320.6	386.1	**341.6**
	58.77	389.2	318.2	384.1	**341.4**
	62.97	362.4	315.5	380.3	**341.1**
	74.28	346.7	311.1	373.3	**340.5**
Ti-H alloy 12at.% H (Senkov and Jonas, 1996)	18.62	209.2	140.6	198.7	**154.4**
	20.64	183.4	134.5	192.8	**153.9**
	23.16	168.2	132.6	186.4	**153.6**
	26.24	146	131.6	183.3	**153.5**
Ti-6Al-4 V (Lavinia et al., 2014) 723 – 873K	226.8	319	254.3	284.0	**267.4**
	242.1	286.9	251.2	284.8	**267.3**
	254.1	267.2	249.3	275.5	**266.9**
	267.3	233.4	246.3	271.2	**266.4**
TiB + La_2O_3 (Lv Xiao et al., 2009) 1123 - 1223 K	169.5	416	337.6	383.9	**354.9**
	177.1	382.4	334.7	382.7	**354.3**
	186.2	365.3	331.6	379.9	**354.1**
	191.7	332.7	327.4	379.9	**353.7**
ZM21 wrought Mg alloy (El Mehtedi et al., 2009)373–423K	108.6	170	162.3	173.4	**149.9**
	113.4	158.2	156.4	166.7	**149.4**
	119.7	134.9	153.4	159.4	**149.1**
	124.6	119.4	151.2	156.3	**148.2**
2.25Cr - 1.6 W Steels (Whittaker and Wilshire, 2010) 773 - 923 K	123.2	435.2	304.2	376.5	**338.7**
	128.3	382.4	301.3	362.9	**338.2**
	141.5	365.8	299.4	348.1	**337.9**
	152.7	331.8	294.5	340.7	**337.1**

Table 11
Error (in%) analysis of the scatter in the values of *Q* for high temperature creep for the four methods.

Systems	Method of Experimental scientists	Improved Method of Experimental scientists	Method of Rheology	Method of Padmanabhan et al., 2015
NiAl-9Mo	14.4	3.0	3.3	**0.3**
Ti-H alloy 12at.% H	35.7	6.6	8.0	**0.6**
Ti-6Al-4 V	30.9	3.1	4.5	**0.4**
TiB + La_2O_3	22.2	3.0	1.0	**0.3**
ZM21 Mg alloy	34.7	7.1	10.4	**1.1**
2.25Cr-1.6 W Steels	27.2	3.2	10.0	**0.5**
Average (%)	**27.6**	**4.4**	**6.3**	**0.5**

High temperature creep: method of experimental scientists

Here the stress is normalised with respect to the shear modulus, *G* of the material, whose value is obtained by the rule of mixtures starting from the values at room temperature of the constituent elements. The effect of change in the value of *n* with temperature is ignored and a mean value is taken for the whole range of temperature involved. The graphical representations are given in Fig. 1 and the real activation energy, *Q* values were calculated for both $\nu = (kT/h)$ and $\nu = 10^{13}\ s^{-1}$ - Table 1. The values within brackets are the mean values of the real activation energy.

Table 12
Steady state superplasticity: Real activation energy for the rate controlling deformation mechanism in case of the 6 systems analysed for both $\nu = (kT/h)$ and $\nu = 10^{13}s^{-1}$.

Systems	Method of Experimental scientists (mean values within parenthesis)	
	Q, [KJ/mol.] $\boldsymbol{\nu = (kT/h)}$	**Q,** [KJ/mol.] $\boldsymbol{\nu = (10^{13}s^{-1})}$
Al–Mg–Sc–Zr alloy (Mengjia et al., 2017) 723–798 K	**93.4 – 163 (128.2)**	**100.8 - 169.68 (134.8)**
Ti-2.5Al-1.8Mn (Mikhaylovskaya et al., 2017) 1088 - 1163K	**112.5 – 188 (150.2)**	**119.5 - 195.05 (157.3)**
Ti-6Al-4 V (Alabort et al., 2016) 1023 - 1173 K	**254.2 - 317.5 (285.8)**	**261.2 - 324.56 (192.9)**
Mg alloy WE43 (Sahithya et al., 2017) 623 – 673 K	**153.2 - 213.4 (183.3)**	**159.7 - 219.91 (189.8)**
TA15 alloy (Sun and Wang, 2014) 1053–1173 K	**243.2 – 324 (283.6)**	**250.2 - 331.06 (290.6)**
High Pb ternary alloy (Harry and Junghyun, 2016) 333 – 423 K	**59.4 – 82 (62.7)**	**65.44 – 88.04 (76.9)**

Table 13
Steady state structural superplasticity: Real activation energy was calculated for both $\nu = (kT/h)$ *and* $\nu = (10)^{-13}s^{-1}$ at constant $(\frac{\sigma(T)}{G(T)})^{n(T)}$.

Systems	Improved Method of Experimental scientists (mean values within parenthesis)	
	Q, [KJ/mol.] $\boldsymbol{\nu = (kT/h)}$	**Q,** [KJ/mol.] $\boldsymbol{\nu = (10^{13}s^{-1})}$
Al–Mg–Sc–Zr alloy (Mengjia Li et al., 2017) 723 −798 K	**105.3 - 111.3 (108.3)**	**111.6 - 117.6 (114.6)**
Ti-2.5Al-1.8Mn (Mikhaylovskaya et al., 2017) 1088 - 1163K	**145.1 - 152.4 (148.7)**	**157.4 - 164.7 (161.5)**
Ti-6Al-4 V (Alabort et al., 2016) 1023 - 1173 K	**273.2 - 280.8 (277)**	**282.3 – 289.9 (286.1)**
Magnesium alloy WE43 (Sahithya et al., 2017) 623 – 673 K	**170.2 - 177.8 (174)**	**175.6 - 183.2 (179.4)**
TA15 alloy (Sun and Wang, 2014)1053 - 1173 K	**216.8 - 226.1 (221.4)**	**226.4 - 235.7 (231.5)**
High Pb ternary alloy (Harry and Junghyun, 2016) 333 – 423 K	**72.3 - 80.2 (76.2)**	**78.8 - 86.7 (82.7)**

Table 14
Steady state structural superplasticity: Calculation of Q for different systems from the apparent activation energy values at constant stress, Q_σ using Eqs. (7)–(10).

Systems	Method of Rheology		
	$\boldsymbol{Q_\sigma}$ *[KJ/mol.]*	**Q,** *[KJ/mol.]* $\boldsymbol{\nu = (kT/h)}$	**Q,** *[KJ/mol.]* $\boldsymbol{\nu = (10^{13}s^{-1})}$
Al–Mg–Sc–Zr alloy (Mengjia Li et al., 2017) 723–798 K	**157.3 – 218.5**	**115.3 – 125.8**	**121.5 – 131.5**
Ti-2.5Al-1.8Mn (A.V. Mikhaylovskaya et al., 2017) 1088 - 1163K	**166.5 – 196.8**	**166.5 – 176.2**	**175.9 – 182.6**
Ti-6Al-4 V (E. Alabort et al., 2016) 1023 - 1173 K	**311.1 – 356.5**	**312.9 – 329.4**	**322.0 – 331.5**
Magnesium alloy WE43 (Sahithya et al., 2017) 623 – 673 K	**156.1 – 180.5**	**158.8 – 167.8**	**164.2 – 173.7**
TA15 alloy (Sun and Wang, 2014)1053–1173 K	**209.7 – 302.2**	**218.8 – 225.2**	**228.1 – 234.5**
High Pb ternary alloy (Harry and Junghyun, 2016) 333 – 423 K	**87.9 – 107.3**	**88.3 – 92.2**	**91.5 – 98.5**

Table 15
$Q_\sigma - \sigma$ relationship and Q values for Ti-2.5Al-1.8Mn alloy (Mikhaylovskaya et al., 2017) obtained using Eqs. (7) and ((9).

Stress, σ[MPa]	Q_σ,[*KJ/mol.*]	*Q,* [*KJ/mol.*]$\nu = (kT/h)$	*Q,* [*KJ/mol.*]$\nu = 10^{13}s^{-1}$
9.12	196.8	197.2	206.6
11.36	188.2	188.6	197.9
15.11	179.9	180.1	189.5
17.79	178.6	178.7	188.1
21.81	166.5	166.5	175.9

In this analysis n is assumed to be independent of temperature, which is not the case (see Fig. 1(c), (d)). As pointed out earlier, the values of G used are less accurate than those obtainable using the regression equations due to Frost and Ashby (Frost and Ashby, 1982). The real activation energy values for the rate controlling process for one alloy, determined at different constant values of $(\frac{\sigma}{G})$, is shown in Table 2 as an example. It is clear that contrary to the requirement of Arrhenius kinetics, the real activation energy values are not constant, but decrease significantly with increasing stress level that is kept constant.

High temperature creep: improved method of experimental scientists

In this method the temperature dependence of n is taken into account (the value of n is calculated as a linear function of T using the method of least squares) and G is calculated using the equations suggested by Frost and Ashby (Frost and Ashby, 1982). When $\nu = (kT/h)$, the real activation energy is obtained at constant $(\frac{\sigma(T)}{G(T)})^{n(T)}$from a plot of $\ln\dot{\varepsilon}$ vs $(1/T)$ (Eq. (11a)), whose slope equals $(-\frac{Q}{k})$. If the analysis were robust, the value of Q obtained should be independent of the magnitude of $(\frac{\sigma(T)}{G(T)})^{n(T)}$ which is kept constant. When $\nu = 10^{13}s^{-1}$, the relation $(\ln\dot{\varepsilon} + \ln T)$ *vs* $(1/T)$ at constant $(\frac{\sigma(T)}{G(T)})^{n(T)}$ should be linear and the slope should again be equal to $(-\frac{Q}{k})$ (Eq. (11b)). The computed values of the real activation energy, Q for the different systems are presented in Table 3.

Value of Q as a function of the value of $(\frac{\sigma(T)}{G(T)})^{n(T)}$*kept constant for NiAl-9Mo (Weili et al., 2004)*

The alloy NiAl-9Mo (Weili et al., 2004) is considered. The stress is normalised by the shear modulus, G (evaluated using the Frost-Ashby (Frost and Ashby, 1982) equations), n is expressed as a function of T and the corresponding values of strain rates were digitized.

When $\nu = (kT/h)$, a plot of $ln\,\dot{\varepsilon}$ vs $(1/T)$ at constant $(\frac{\sigma(T)}{G(T)})^{n(T)}$ (Fig. 2) has a slope of $(-\frac{Q}{k})$ from which one obtains the values of Q at different values of $(\frac{\sigma(T)}{G(T)})^{n(T)}$, which are shown in Table 4. Similarly, when using the relation $\nu = 10^{13}s^{-1}$, a plot of $(\ln\dot{\varepsilon} + \ln T)$ *vs* $(1/T)$ at constant $(\frac{\sigma(T)}{G(T)})^{n(T)}$ is made, the slope of which gives the value of $(-\frac{Q}{k})$.

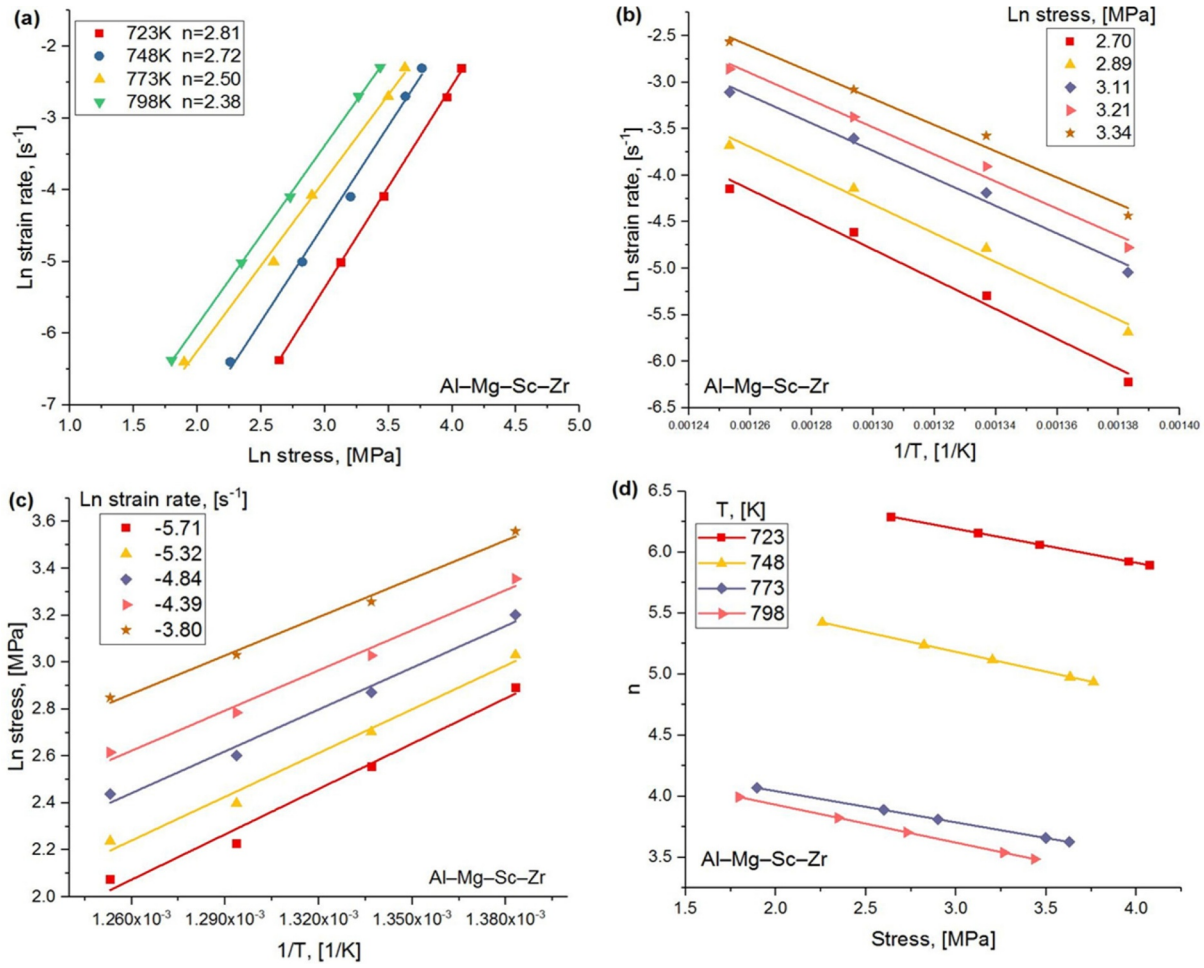

Fig. 7. Plots pertaining to the system Al-Mg-Sc-Zr (Mengjia et al., 2017) and the determination of real activation energy value from Q_σ and $Q_{\dot{\varepsilon}'}$ values obtained using Eqs. (7)–(10).

It is seen that the scatter in the values of Q in this method at different values of $(\frac{\sigma(T)}{G(T)})^{n(T)}$ is much smaller than in the previous method.

High temperature creep: the method of rheology

In the method of rheology the value of Q is obtained from the apparent activation energies determined at constant stress, Q_σ and constant strain rate $Q_{\dot{\varepsilon}}$ (McKelvey, 1962). Stress is not normalized in this procedure. The values of Q, Q_σ *and* $Q_{\dot{\varepsilon}}$ for the 6 systems were determined using Equations ((3) - (6). The findings are reported in Table 5.

Detailed results of $Q_\sigma - \sigma$, and $Q_{\dot{\varepsilon}} - \dot{\varepsilon}$ relationships and Q values computed at different stress levels by the method of rheology for Ti-6Al-4 V (Lavinia et al., 2014) and NiAl-9Mo (Weili et al., 2004) are presented in Tables 6 and 7. In addition, graphical representation of the estimations for two other materials (in situ TiB_2 + La_2O_3 and 2.25Cr – 1.6 W Steels) are shown in Figs. 3(a)–(f) and 4(a)–(f).

Scatter in the predictions in this method is quite large.

High temperature creep: method of Padmanabhan et al. (2015)

Using Eqs. (11a) and (11b) ($\nu = (kT/h)$ and $\nu = 10^{13}s^{-1}$ respectively), the values of the real activation energy for the 6 systems were calculated and the results are presented in Table 8.

As in the earlier paper (Padmanabhan et al., 2015), the values of $ln\,\dot{\varepsilon}$ were predicted at different stresses for both $\nu = (kT/h)$ and $\nu = 10^{13}\,s^{-1}$. The results for the stress versus the predicted and experimental strain rates for 4 systems are presented in Fig. 5. The results are very consistent. Similarly, the values obtained for the real activation energy, Q are practically independent of the values of the stress at which they are obtained and these are reported in Table 9.

The value of Q is nearly independent of the different values of $n_0(\ln\sigma - \ln\sigma_r)$ *that is kept constant: Ti-H alloy 12at.% H (Senkov and Jonas, 1996) (see Table. 9).*

From Padmanabhan et al. (2015) as well as the summary presented above it follows that

$$n_{01}(\ln\sigma_1 - \ln\sigma_r) = n_{02}(\ln\sigma_2 - \ln\sigma_r) = n_{03}(\ln\sigma_3 - \ln\sigma_r)$$

Here σ_r is the reference stress which is taken as the maximum stress employed in the experiment, *i. e.*, $\sigma_r = 45.11\ MPa$ for this system. The numerical suffixes denote different temperatures.

When, $\nu = (kT/h)$ a plot of $ln\,\dot{\varepsilon}$ vs $(1/T)$ at constant $n_0(\ln\sigma - \ln\sigma_r)$ (Fig. 6) is plotted, the slope of which equals $(-\frac{Q}{k})$, from which Q ranging from 153.3 to 154.4 *KJ/mol.* is obtained at different levels of constant $n_0(ln\ \sigma - ln\ \sigma_r)$ values. That is, the value of Q is practically independent of the magnitude of $n_0(\ln\sigma - \ln\sigma_r)$ that is kept constant. Similarly, when $\nu = 10^{13}s^{-1}$, a plot of $(\ln\dot{\varepsilon} + \ln T)$ *vs* $(1/T)$ at constant $n_0(\ln\sigma - \ln\sigma_r)$ is plotted, the slope of which, once again, is equal to $(-\frac{Q}{k})$. In this method the value of Q ranges from $160.5 - 161.3KJ/mol.$, i.e., it is practically independent of the magnitude of $n_0(\ln\sigma - \ln\sigma_r)$.

3.2. Effect of grain size on power law creep

It has been reported in several studies that when dislocation processes dominate, grain size practically has no effect on creep

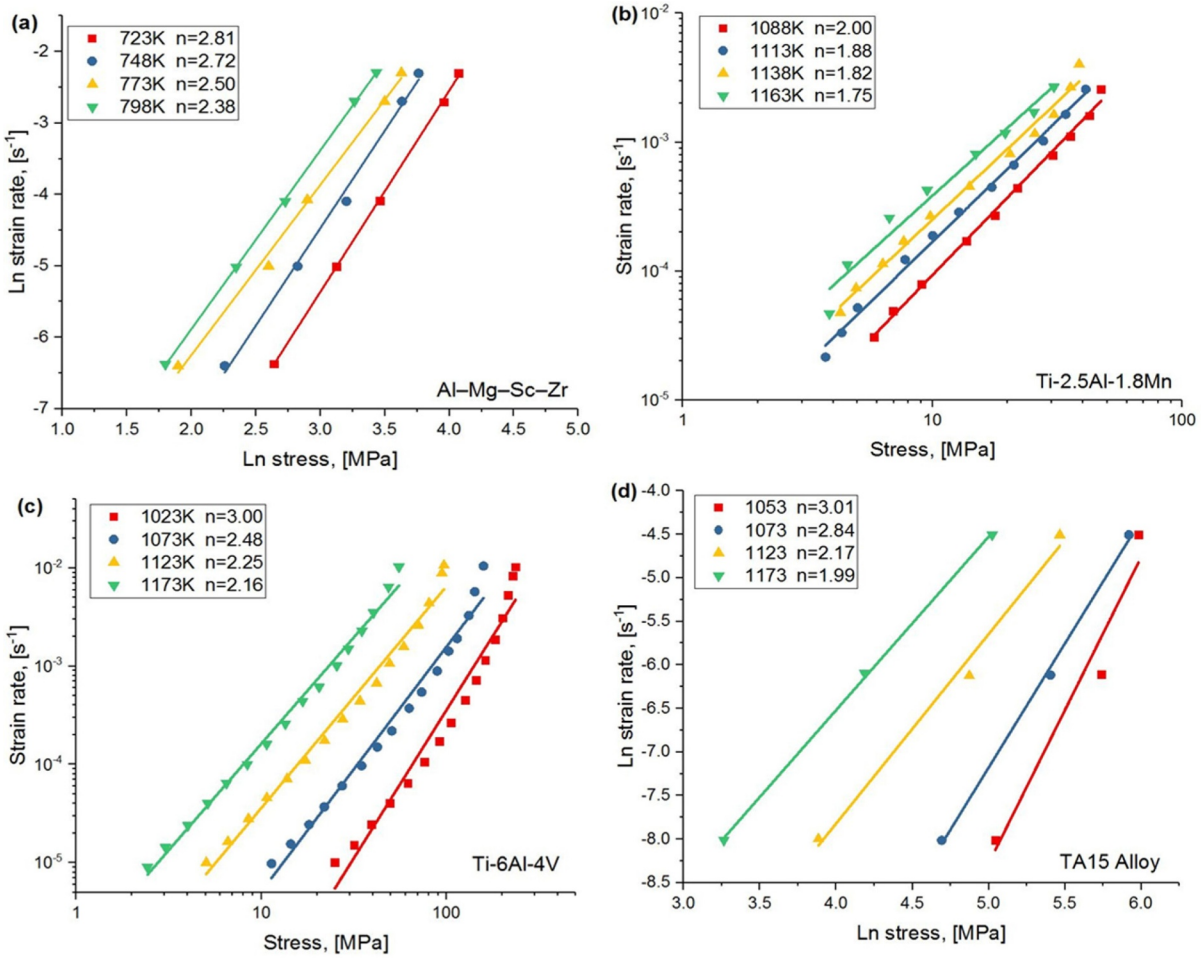

Fig. 8. Plots of strain rate vs. stress relationship. The plots correspond to the data digitized. The above four plots correspond to (a) Al–Mg–Sc–Zr alloy of 4.4 μm grain size (Mengjia et al., 2017), (b) Ti-2.5Al-1.8Mn alloy of 7.2 μm grain size (Mikhaylovskaya et al., 2017), (c) Ti-6Al-4 V alloy of grain size 6.1 μm (Alabort et al., 2016), (d) TA15 alloy of grain size 2 μm (Sun and Wang, 2014).

deformation, e.g. Mannan and Rodriguez, 1983. For example, the creep rate for grain sizes of 0.040 mm and 0.650 mm in AISI type 316 stainless steel was investigated at 873 and 973 K at different stresses. Power law creep was observed and the effect of grain size on the creep rate was negligible (Mannan and Rodriguez, 1983). In another study of flexural creep response at 1200° and 1300 °C of alumina reinforced with 10 vol.% SiC whiskers, wherein the grain size was varied from 1.2 to 8.0 μm, it was found that the creep rate was insensitive to grain size (Lin et al., 1996).

3.3. Comparison of results obtained by different methods for high temperature creep

The values of Q ($for\ \nu = kT/h$) at different constant stress levels obtained for all systems considered using the different methods are compared in Table 10.

3.4. Error analysis: high temperature creep

Table 10 presents an analysis of the scatter present in the values of the real activation energy predicted by the four methods.

From the values given in Table 10, the error for every method is analysed using the relation given in Eq. (15) and the values are reported in Table 11.

$$Error = \left(\frac{Highest\ \ value - Lowest\ \ value}{Mean\ \ value}\right) \times 100\% \tag{15}$$

From the above analysis it is clear that an average error of ± 0.5% (maximum error of 1.1%) is present in the method of Padmanabhan et al. (2015), which is the lowest value and thus this analytical procedure is seen to be the most accurate. The improved method of experimental scientists (average error 4.4%; maximum error 7.1%) is the second most accurate. The percentage error of the method of experimental scientists is rather high and its usage could be avoided in the interest of precision.

3.5. Steady state structural superplasticity

In case of steady state structural Superplasticity data concerning 6 more systems were analysed. The chosen systems are: Al–Mg–Sc–Zr alloy of 4.4 μm grain size (Mengjia et al., 2017), Ti-2.5Al-1.8Mn alloy of 7.2 μm grain size (Mikhaylovskaya et al., 2017), Ti-6Al-4 V alloy of grain size 6.1 μm (Alabort et al., 2016), Magnesium alloy WE43 of 2 μm grain size (Sahithya et al., 2017), TA15 alloy of grain size 2 μm (Sun and Wang, 2014) and High Pb ternary alloy of 4.2 μm grain size (Harry and Junghyun, 2016) (Fig. 8). As before, an analysis was carried out using the four methods.

Steady state structural superplasticity: the method of experimental scientists

The real activation energy for the rate controlling process, Q for the systems was calculated using Eq. (1), treating m to be independent of T and $\dot{\varepsilon}/\sigma$. The results are presented in Table 12.

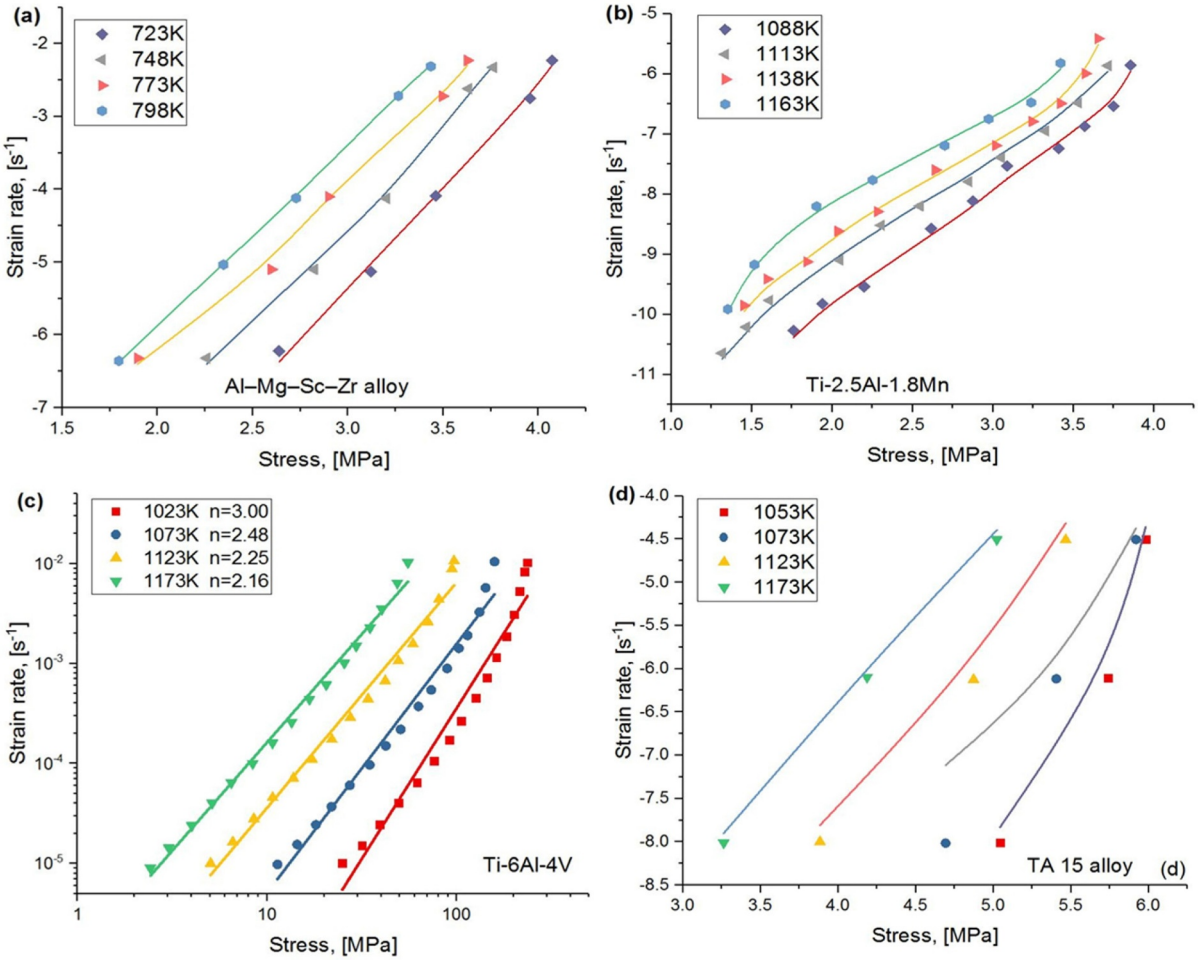

Fig. 9. Double logarithmic plots of stress vs. strain rate curves. The symbols represent the experimental points and the curves are based on the developed equations. The four systems considered are: (a) Al–Mg–Sc–Zr alloy of 4.4 μm grain size (Mengjia et al., 2017), (b) Ti-2.5Al-1.8Mn alloy of 7.2 μm grain size (Mikhaylovskaya et al., 2017), (c) Ti-6Al-4 V alloy of grain size 6.1 μm (Alabort et al., 2016) and (d) TA 15 alloy of 2 μm grain size (Sun and Wang, 2014).

Steady state structural superplasticity: the improved method of experimental scientists

The values of real activation energy was calculated keeping $(\frac{\sigma(T)}{G(T)})^{n(T)}$ as constant. G was calculated as a linear function of temperature using the Frost-Ashby equations (Frost and Ashby, 1982). The activation energy values calculated by the improved method of experimental scientists for the 6 systems are reported in Table. 13.

Steady state structural superplasticity: the method of rheology

Using Eqs. (7)–(10) the value of real activation energy, Q was calculated from the $Q_\sigma$values for every system. The results are reported in Table 14. As an example, in Table 15 the calculated values of Q from the apparent activation energy values determined at different constant stresses, Q_σ in the temperature range 1088K-1163 K in case of Ti-2.5Al-1.8Mn alloy (Mikhaylovskaya et al., 2017) are presented. The computation was repeated with all the alloys considered.

The predictions pertaining to the experimental data of Al–Mg–Sc–Zr alloy of grain size 4.4 μm at temperatures of 723–798 K are presented in Fig. 7. The calculations are based on Eqs. (7)–(10). The experimental points are given as symbols.

Steady state structural superplasticity: the method of Padmanabhan et al. (2015)

The same 6 systems were analysed using Eqs. (12)–(14). From Eq. (13) it follows that at a given temperature $p_0 = (B-1)$ and $\sigma_c = (p_0/C)$. The following facts should be noted. (a) For obtaining the predictive equation for the variation of n as a function of T, the method of least squares was used, and (b) experimentally, it is known that p_0, σ_c and n decrease with increasing T. These facts give rise to two constraints: i.e., (i) B in Eq. (14)/ (14a) should decrease with increasing T, and (ii) In Eq. (14) under isothermal conditions (see derivation) $p_0 = (C.\sigma_c)$. That is, (C_i/C_{i-1}) should always be equal to $(p_{0i}/p_{0(i-1)}) \times (\sigma_{c(i-1)}/\sigma_{ci})$, where the subscripts (i) and $(i-1)$ correspond to two different temperatures T_i and T_{i-1}; C, p_0 and σ_c values mentioned along with the subscripts correspond to the values of these parameters at each of the two temperatures (Padmanabhan et al., 2015).

In addition, using the experimental values of $ln\,\sigma - ln\,\dot{\varepsilon}$ digitized for different temperatures and Eqs. (11) and (11a), the values of Q, A_3 and A_4 were determined. With these values, $ln\,\dot{\varepsilon}$ values at different temperatures and stresses are computed for $\nu = (kT/h)\ and\ \nu = 10^{13}s^{-1}$. Clearly, the experimental and the computed values agree very well.

The $ln\,\dot{\varepsilon}$ values which are calculated for the four systems are compared in a plot with the experimental $ln\,\dot{\varepsilon}$ values - see Fig. 9.

Among the four methods considered here a prediction this analysis alone is capable of making is that during optimal structural Superplasticity the stress exponent, n decreases linearly with increasing stress σ (Eq. (13)). This relationship is verified/ validated in Fig. 10 for four systems chosen randomly as examples.

In addition, the real activation energy, Q for the rate controlling mechanism was calculated for both $\nu = (kT/h)$ and $\nu = 10^{13}s^{-1}$. These values are presented in Table 16.

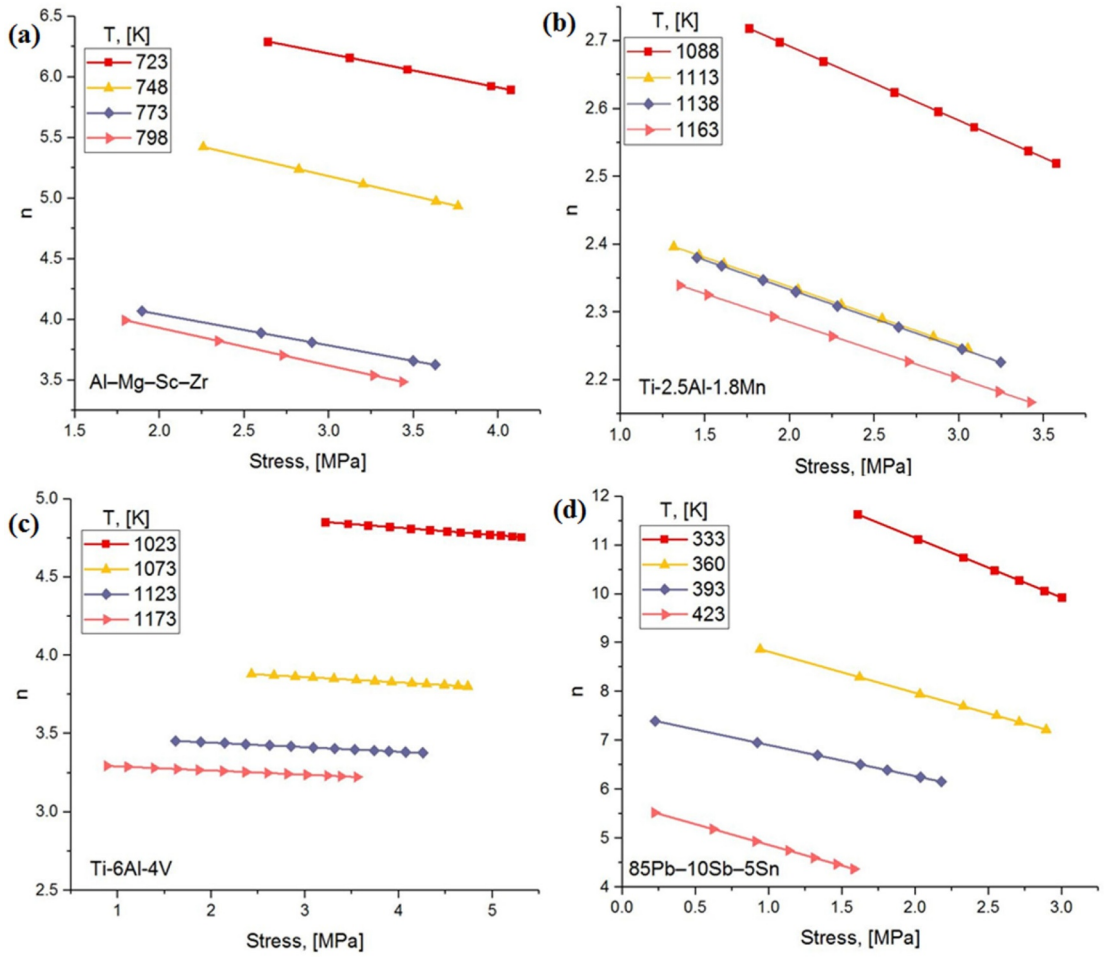

Fig. 10. Validation of the prediction that n vs. stress at constant temperature is linear: (a) Al–Mg–Sc–Zr alloy of 4.4 μm grain size (Mengjia et al., 2017), (b) Ti-2.5Al-1.8Mn alloy of 7.2 μm grain size (Mikhaylovskaya et al., 2017), (c) Ti-6Al-4 V alloy of grain size 6.1 μm (Alabort et al., 2016), (d) High Pb ternary alloy of 4.2 μm grain size (Harry and Junghyun, 2016).

Table 16
Steady state structural superplasticity: Real activation energy for the rate controlling deformation mechanism in case of the 6 systems for both $\nu = (kT/h)$ and $\nu = 10^{13}\ s^{-1}$.

Systems	Padmanabhan et al., 2015 (mean values within parenthesis)	
	***Q**, [KJ/mol.]* $\nu = (kT/h)$	***Q**, [KJ/mol.]* $\nu = (10^{13}s^{-1})$
Al–Mg–Sc–Zr alloy (Mengjia et al., 2017) 723–798 K	**116.2 - 117.5** (116.5)	**122.5 - 123.8** (123.1)
Ti-2.5Al-1.8Mn (Mikhaylovskaya et al., 2017) 1088 - 1163K	**165.2 - 166.8** (166)	**173.5 - 175.1** (174.3)
Ti-6Al-4 V (Alabort et al., 2016) 1023 - 1173 K	**292.6 - 293.9** (293.2)	**301.9 - 303.2** (302.5)
Mg alloy WE43 (Sahithya et al., 2017) 623 – 673 K	**154.9 - 156.1** (155.5)	**160.3 - 161.5** (160.9)
TA15 alloy (Sun and Wang, 2014) 1053–1173 K	**212.4 - 214.5** (213.4)	**221.6 - 223.7** (222.6)
High Pb ternary alloy (Harry and Junghyun, 2016)333 – 423 K	**86.7 - 87.9** (87.3)	**89.9 - 91.15** (90.5)

It is clear that the entire region of steady state superplasticity can be accounted for using a single real activation energy value for the rate controlling mechanism. Importantly, these real activation energy values are very close to those reported for Grain Boundary Sliding (GBS) (Padmanabhan and Davies, 1980; Kaibyshev, 1992) and computed theoretically and verified experimentally by Sripathi and Padmanabhan (2014).

3.6. Comparison of the four methods for steady state superplasticity

The real activation energy values for the different systems computed by the four methods are reported in Table 17.

3.7. Error analysis

The scatter in the computed values of the real activation energy as a function of the stress level maintained constant was analysed and compared for the four methods. The findings are reported in Table 18. The computations for the four methods can be carried out for both the values of ν ($\nu = kT/h$ and $\nu = 10^{13}s^{-1}$). (To conserve space, in this paper, in Tables 10, 11, 17 and 18 the values computed for $\nu = kT/h$ alone are presented.)

Here again the method of Padmanabhan et al. (2015) is the most accurate, which is followed by the improved method of experimental scientists. The levels of accuracy obtainable in the other two methods

Table 17
Consistency analysis for steady state structural superplasticity. Comparison of the real activation energy values for the different systems at various stress levels.

Systems	Constant Stress Levels [MPa]	Method of Experimental scientists **Q**, *[KJ/mol.]*	Improved Method of Experimental scientists **Q**, *[KJ/mol.]*	Method of Rheology **Q**, *[KJ/mol.]*	Method of Padmanabhan et al., 2015 **Q**, *[KJ/mol.]*
Al–Mg–Sc–Zr alloy (Mengjia et al., 2017)723 – 798 K	0.94	163	111.3	125.1	**117.5**
	1.32	139.8	109.4	122.0	**117.3**
	1.70	112.4	107.1	118.9	**117.1**
	2.13	93.4	105.3	118.1	**116.2**
Ti-2.5Al-1.8Mn (Mikhaylovskaya et al., 2017) 1088 - 1163K	9.12	188	152.4	197.2	**166.8**
	11.32	165.4	150.2	188.6	**166.6**
	15.11	134.8	146.8	180.1	**166.1**
	17.79	112.5	145.1	178.7	**165.2**
Ti-6Al-4 V (Alabort et al., 2016) 1023 - 1173 K	26.16	317	280.8	359.4	**293.9**
	32.27	287.5	278.3	347.6	**293.4**
	41.48	265.4	276.1	330.9	**293**
	47.62	254.2	273.2	322.0	**292.6**
Magnesium alloy WE43 (Sahithya et al., 2017) 623 – 673 K	23.90	213.4	177.8	180.8	**156.1**
	26.82	187.9	174.2	173.9	**156**
	29.81	176.3	172	168.6	**155.7**
	34.16	153.2	170.2	163.9	**154.9**
TA15 alloy (Sun and Wang, 2014)1053 - 1173 K	158.17	324	226.1	310.2	**214.5**
	171.44	298.3	221.4	257.1	**214.2**
	191.35	264.2	219.4	247.8	**214**
	211.37	243.2	216.8	230.1	**212.4**
High Pb ternary alloy (Harry and Junghyun, 2016) 333 – 423 K	6.32	82	80.2	107.2	**87.9**
	7.27	64.3	79.2	105.9	**87.8**
	9.24	63.2	76.3	99.7	**87.1**
	10.6	59.4	72.3	94.3	**86.7**

Table 18
Analysis of scatter (in%) in the values of Q obtained by the four methods.

Systems	Method of Experimental scientists	Improved Method of Experimental scientists	Method of Rheology	Method of Padmanabhan et al., 2015
Al–Mg–Sc–Zr alloy	54.7	5.5	5.7	**1.1**
Ti-2.5Al-1.8Mn	50.2	4.9	9.9	**0.9**
Ti-6Al-4V	22.3	2.7	11.0	**0.4**
Magnesium alloy WE43	32.9	4.3	9.8	**0.7**
TA15 alloy	28.6	4.2	30.6	**0.9**
High Pb ternary alloy	33.6	10.2	12.6	**1.3**
Average (%)	**22.3 - 54.7 (37.1)**	**2.7 - 10.2 (5.3)**	**5.7 - 30.6 (13.4)**	**0.4 - 1.3 (0.9)**

are not satisfactory, particularly in the method of experimental scientists.

3.8. Effect of grain size on steady state superplasticity

Steady state superplastic flow is strongly influenced by grain size (Padmanabhan and Davies, 1980; Ghosh and Raj, 1981; Kaibyshev, 1992; Imayev et al., 1997; Li et al., 2017). In the earlier paper (Padmanabhan et al., 2015) the grain size exponent in terms of the Buckingham Pi Theorem (White, 2011) [please see Appendix. 1 for details] was not determined. This task is completed here. Four systems were analysed using the stress-strain rate relationship corresponding to different grain sizes at a given temperature. The systems chosen are: Al–Mg–Sc alloy of 1.6, 2.6 and 2.9 μm grain sizes at temperatures in the range of 673 – 798 K (Liu and Ma, 2011), Mg-Zn-Y-Zr alloy of 2, 5 and 10 μm grain sizes at temperatures in the range of 573 – 673 K (Tang et al., 2009), AZ91 alloy of grain sizes 1.2, 3.1 and 7.8 μm at temperatures in the range of 523 – 648 K (Chai et al., 2013), and Mg-3Gd-1 Zn alloy of 1.7, 4.9 and 8.2 μm grain sizes at temperatures in the range of 573 – 723 K (Sarebanzadeh et al., 2015). The reference grain size chosen for normalizing the grain sizes was 20 μm.

Considering together the 4 alloys examined here the grain size dependence of superplastic strain rate in the method of Padmanabhan et al. (2015) is (−1.19), with individual values for different systems falling in the range of 1.33 to 0.96. The material-agnostic maximum scatter in the mean grain size exponent is ± 0.37. From Table 19 it is clear that this is the most accurate of the four methods examined in this study. The improved method of experimental scientists with a maximum scatter of ± 0.41 is a close second. The scatter in the method of experimental scientists is rather large and the use of this technique should be viewed with caution. A final point: In the method of Padmanabhan et al. (2015) for obtaining normalized grain sizes of value less than unity, the grain size is divided by a large grain size, 20 μm. As superplastic strain rate is inversely related to the grain size, the grain size exponent for this method always has a negative value.

The strain rate – grain size relationship at every temperature is plotted on a log-log scale. From the slope of the resultant straight lines, the grain size exponent values are determined. Fig. 11 shows, as an example for a single system, how the strain rate varies with grain size at different temperatures.

Evidently the temperature dependence of the grain size exponent is the least for the method of Padmanabhan et al., 2015. The findings for all the four systems are summarised in Table 19.

4. Concluding remarks

4.1. High temperature creep

The effectiveness and accuracy of prediction possible with the four methods is now examined material-wise.

(i) Ti – 12 at.% H alloy (Senkov and Jonas, 1996): The system was tested by the original authors in the temperature range of

Table 19
Comparison of grain size exponent for the 4 systems obtained using the 4 methods.

Systems	Constant Stress levels [MPa]	At different Temperature [K]	Method of Experimental scientists	Improved Method of Experimental scientists	Method of Rheology	Method of Padmanabhan et al., 2015
			(mean values within parenthesis)			
			Grain size exponent, a	**Grain size exponent, a**	**Grain size exponent, a**	**Grain size exponent, a**
Al–Mg–Sc alloy (F. C. Liu et al., 2011) 673–798 K	25.24	673	1.76	1.53	1.72	−0.89
		698	0.77	1.48	1.41	−0.92
		723	0.56	1.32	1.28	−0.98
		748	0.43	1.17	1.02	−1.08
			(0.88)	**(1.37)**	**(1.35)**	**(−0.96)**
Mg–Zn–Y–Zr alloy (W.N. Tang et al., 2009) 573 - 673K	11.48	573	1.84	1.89	1.13	−1.25
		598	0.85	1.84	0.82	−1.29
		623	0.24	1.68	0.68	−1.36
		673	0.12	1.53	0.42	−1.45
			(0.76)	**(1.73)**	**(0.76)**	**(−1.33)**
AZ91 Magnesium alloy (Fang Chai et al., 2013) 523 - 648 K	36.43	523	1.64	1.73	1.24	−1.16
		573	0.76	1.68	0.93	−1.21
		623	0.24	1.52	0.80	−1.27
		648	0.14	1.37	0.54	−1.36
			(0.69)	**(1.57)**	**(0.87)**	**(−1.25)**
Mg-3Gd-1 Zn **alloy (M. Sarebanzadeh et al., 2015) 573 – 723 K**	121.5	573	1.98	1.24	1.65	−1.14
		623	1.79	1.19	1.34	−1.18
		673	1.38	1.04	1.21	−1.25
		723	1.26	0.88	0.94	−1.34
			(1.65)	**(1.32)**	**(1.28)**	**(−1.22)**
Maximum scatter in the mean value foreach method if considered in a material-agnostic sense	±	±	± 0.96	± 0.41	± 0.59	± 0.37

973–1233 K. Here it is analysed by the three methods of method of experimental scientists, improved method of experimental scientists and the analysis due to Padmanabhan et al. (2015). As the method of rheology leads to a large scatter in the predictions (see earlier portions) and it is also not consistent with the tenets of the Buckingham Pi Theorem, it is not considered any further.

The activation energy values obtained by the three methods are shown in Table 20. In the method of experimental scientists, the scatter in the predicted value is large and the total temperature interval has to be divided into two sub-domains with two different rate controlling mechanisms. In this sense this is a less useful method compared with the other two in which the scatter in the predicted values are of a very small magnitude and the whole temperature range could be covered by a single rate controlling mechanism. To decide between the magnitudes of the activation energy values obtained by the two methods, one will have to use microstructural and topological evidence to identify the physical mechanism, which controls the rate of deformation. But even at this stage it is safe to note that the activation energy values obtained by the two techniques, viz. improved method of experimental scientists and the one due to Padmanabhan et al. (2015) are rather close.

(ii) Ti-6Al-4V (Lavinia et al., 2014): The following comments are significant. The $\ln \dot{\varepsilon} - \ln \sigma$ plots cover a temperature range of 723 – 873 K.

The activation energy values corresponding to the three methods are presented in Table. 21. All the points made concerning the first system are valid here also. But in this case the scatter is less in the improved method of experimental scientists compared with that of Padmanabhan et al. (2015), even though the scatter is rather small in both the cases in absolute terms.

For the systems NiAl-9Mo (Weili et al., 2004) in the temperature range 1123 - 1223 K, TiB + La2O3 (Lv Xiao et al., 2009) in the range 1123 - 1223 K, ZM21 wrought Mg alloy (El Mehtedi et al., 2009) in the temperature range 373–423 K, 2.25Cr - 1.6 W Steel (Whittaker and Wilshire, 2010) in the temperature range 773 - 923 K considered in this paper, the activation energy values obtained by the respective authors are: 346.7 – 401, 332.7 – 416, 119.4 – 170 and 331.8 – 435.2 $KJ\ mol^{-1}$ respectively for the whole range of temperature. These values are similar to the values obtained by the method of experimental scientists in this paper. By the method of Padmanabhan et al. (2015) an accurate set of activation energy values of 341, 354.3, 149 and 337.9 $KJ\ mol^{-1}$ is obtained respectively. The activation energy values obtained by the improved method of experimental scientists (315.8, 332.5, 156.7 and 299.3 $KJ\ mol^{-1}$ respectively) are also close to the values obtained using the procedure of Padmanabhan et al. (2015). The inferences concerning the analyses of these four alloys are also very similar to those of the first two alloys discussed earlier.

The numerous analyses of creep data available from the beginning of creep research (see, for example, Dorn, 1955; Harper and Dorn, 1957; Mukherjee et al., 1969; Sherby et al., 1957) have mostly used the method of experimental scientists. They can be rationalized better and keener insights into the rate controlling mechanisms obtained if one were to use the improved method of experimental scientists or the one advocated by Padmanabhan et al. (2015). As pointed out by the latter authors, errors in the prediction of observed strain rates by the improved method of experimental scientists are likely to be larger compared with those found with the technique of Padmanabhan et al. (2015) because in the former method the stress is normalized by the shear modulus, which being more than 1000 times larger than the flow stress, considerably contracts the total strain rate range and as a result leads to a loss of accuracy.

4.2. Steady state structural superplasticity

Here also the results of the method of experimental scientists, improved method of experimental scientists and the one due to Padmanabhan et al. (2015) are discussed.

(i) Al–Mg–Sc–Zr alloy (Mengjia et al., 2017): Temperature range covered is 723 - 773 K and the authors have used the method of

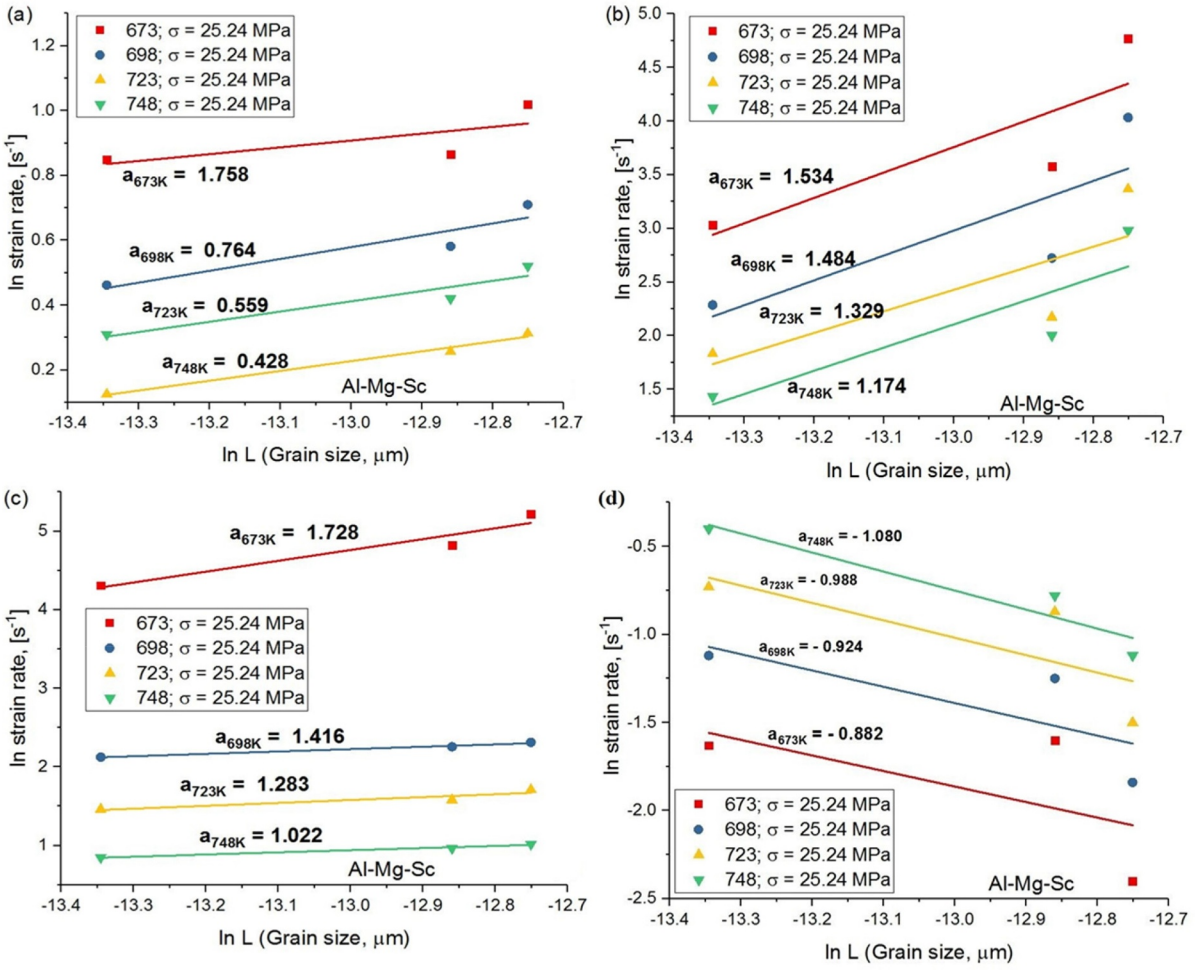

Fig. 11. Plot of ln strain rate (s^{-1}) vs ln grain size (μm) for the Al-Mg-Sc alloy of varying grain sizes (1.6 μm, 2.6 μm, 2.9 μm). (a) Method of experimental scientists, (b) Improved method of experimental scientists, (c) Method of rheology, and (d) Method of Padmanabhan et al., 2015.

Table 20
The activation energy, Q, computed by three different methods for Ti – 12 at.% H alloy.

Method	Zone	Mechanism	Activation Energies [$KJ.\ mol^{-1}$]
Method of Experimental Scientists (Senkov and Jonas, 1996)	973 K – 1073 K	Bulk diffusion in β titanium	130 - 172
	1073 K – 1233 K	Self-diffusion and high-temperature deformation of β titanium	190 - 260
Improved Method of Experimental Scientists	973 K – 1233 K	Can be explained by a single mechanism as rate controlling in the whole range of temperature	131 – 140.6
Method of Padmanabhan et al., 2015	973 K – 1233 K	Can be explained by a single mechanism as rate controlling in the whole range of temperature	154.4–163.7

Table 21
The activation energy values computed by the three methods for Ti-6Al-4 V.

Method	Zone	Mechanism	Activation Energies [$KJ.\ mol^{-1}$]
Method of Experimental Scientists (Lavinia et al., 2014)	723 K – 793 K	Ti self-diffusion and Al solute diffusion	251 - 290
	793 K – 873 K	Controlled by dislocation climb due to lattice diffusion assisted by pipe diffusion	296 - 326
Improved Method of Experimental scientists	723 K – 873 K	Is explained by a single mechanism	256 - 261
Method of Padmanabhan et al., 2015	723 K – 873 K	Is explained by a single mechanism	264 – 277.6

experimental scientists.

(ii) Ti-2.5Al-1.8Mn alloy (Mikhaylovskaya et al., 2017):

Here also the authors have used the method of experimental scientists.

Clearly, from the values of the activation energy shown in Tables 22 and 23, it is clear that the method of Padmanabhan et al. (2015) and the improved method of experimental scientists are better than the method of experimental scientists, which requires two rate controlling mechanisms to account for the observations in the whole temperature

Table 22
The activation energy values computed by the three different methods for Al–Mg–Sc–Zr alloy.

Method	Zone	Mechanism	Activation Energies [$KJ.\ mol^{-1}$]
Method of Experimental scientists (Mengjia et al., 2017)	723 – 773 K	Grain boundary self-diffusion of Al	84.4 – 98.4
	773 – 798 K	Grain boundary sliding	100.8 – 154.2
Improved Method of Experimental scientists	723 – 798 K	Can be explained by a single rate controlling mechanism	105.3 – 111.3
Method of Padmanabhan et al., 2015	723 – 798 K	Can be explained by a single rate controlling mechanism	116.2 – 117.5

Table 23
The activation energy values computed by the three different methods for Ti-2.5Al-1.8Mn alloy.

Method	Zone	Mechanism	Activation Energies [$KJ.\ mol^{-1}$]
Method of Experimental scientists (Mikhaylovskaya et al., 2017)	1088 – 1138 K	Grain boundary self -diffusion	153 - 183
	1138 – 1163 K	Intragranular diffusion	306 - 317
Improved Method of Experimental scientists	1088 – 1163 K	Can be explained by a single rate controlling mechanism	145.1 – 152.4
Method of Padmanabhan et al., 2015	1088 – 1163 K	Can be explained by a single rate controlling mechanism	165.2 – 171.5

range compared with the first two which require only one (rate controlling mechanism). However, the first method has a smaller scatter in the predicted activation energy values and has a better stress normalising procedure than the improved method of experimental scientists.

The activation energy values for the four other systems (Ti-6Al-4 V, Mg alloy WE43, TA15 alloy and High Pb ternary alloy) also show a wide scatter when the method of experimental scientists is used. The activation energy values obtained by the improved method of experimental scientists are very close to those obtained by the method of Padmanabhan et al. (2015). These activation energy values can be identified with that for Grain Boundary Sliding (GBS) in the four alloys (Alabort et al., 2016; Harry and Junghyun, 2016; Sahithya et al., 2017; Sun and Wang, 2014).

Finally, using the Buckingham Pi Theorem for the first time the mechanical response of four superplastic alloys were analysed to obtain a numerical value for the grain size exponent in the superplastic strain rate equation. The grain size exponent obtained in this fashion is consistent with those reported after extensive searches of literature by Padmanabhan and Davies (1980) and Padmanabhan et al. (2018).

Novelty statement

A procedure for improving the accuracy of prediction of the method of materials scientists that analyses creep deformation using the “power law” by including the variations in the value of the strain-rate sensitivity index, m, with temperature (and also with grain size in case of Superplasticity) and estimating the shear modulus at any given temperature in terms of the Frost-Ashby equations is presented. It is shown that this modified method predicts values for the activation energy for the rate controlling process and the strain rate of deformation that are almost as accurate as those predicted by the procedure due to Padmanabhan et al. (2015). It is further shown that the accuracy obtainable by the latter method is better because of its superior way of normalizing the stress term in the strain rate equation to make it consistent with the Buckingham Pi Theorem. It is demonstrated that both these methods are consistent with the tenets of Dimensional Analysis. A power law analysis commonly used in the field of rheology is shown to be inconsistent with the principles of Dimensional Analysis and the least accurate among the different methods of handling the power law strain rate equation for steady state, uniaxial, low stress, high homologous temperature deformation. The above conclusions are verified/validated by analysing the experimental data pertaining to several systems.

Declaration of Competing Interest

The authors declare that they have no known competing financial interests or personal relationships that could have appeared to influence the work reported in this paper.

Acknowledgements

This work is supported by the Confederation of Indian Industry(CII), Science and Engineering Research Board (SERB), Government of India (SERB/PM Fellow/CII – FICCI/Meeting/2018) and the Industry Partner Fifth Generation Technologies(5G Technologies), Chennai, under the scheme of Prime Minister's Fellowship for Doctoral Research, Government of India.

Appendix 1

The Buckingham Pi Theorem is based on the ‘method of dimensions’, first proposed by Lord Rayleigh (1877) (Rayleigh, 1877) and is based on the ideas of matrix algebra and the concept of the ‘rank’ of non-square matrices. The theorem was outlined in 1914 (Buckingham, 1914) using dimensionless parameters.

The theorem

Let $q_1, q_2, q_3 \ldots q_n$ be n dimensional variables that are physically relevant to a given problem and inter-related by a dimensionally homogeneous set of equations. These can be expressed via a functional relationship of the form,

$F(q_1, q_2, \ldots q_n) = 0$, or equivalently $q_1 = f(q_2, \ldots q_n)$

If k is the number of fundamental dimensions required to describe the n variables, then there will be k primary variables and the remaining $j = (n - k)$ variables can be expressed as $(n - k)$ dimensionless and independent quantities or ‘Pi groups’, $\Pi_1, \Pi_2 \ldots \Pi_{n-k}$ $\Pi_1, \Pi_2 \ldots \Pi_{n-k}$. The functional relationship then reduces to the form:

$\phi(\Pi_1, \Pi_2 \ldots \Pi_{n-k}) = 0$, or equivalently $\Pi_1 = \phi(\Pi_2 \ldots \Pi_{n-k})$

This set of dimensionless parameters is not unique. They are, however, independent and form a complete set.

The main advantage of using the Buckingham Pi Theorem is that it reduces the number of variables by combining dimensional variables to form dimensionless parameters. By far the simplest and the most desirable method is that of direct mathematical solution. Therefore, this is one of the powerful techniques, potentially useful for any experimental study (White, 2011).

This analysis is useful in both analytical and experimental work. Some of the advantages are:

1. Checking the dimensional homogeneity of any equation of a physical model.
2. Deriving equations expressed in terms of dimensionless parameters to show the relative significance of each parameter.
3. Planning tests and presenting experimental results in a systematic manner.

In Padmanabhan et al. (2015), where the Buckingham Pi Theorem is used, each dimensional variable is divided by a larger value of the same variable, resulting in a dimensionless quantity of magnitude less than unity. Hence the problem of convergence is avoided, if the function were to be expanded in a power series.

Dimensional analysis/ the Buckingham Pi Theorem finds application in many areas, e.g. fluid mechanics (White, 2011), metrology (Esnault-Pelterie, 1950), astrophysics (Kurth, 1972), engineering (Nag, 2006), chemical processing (Zlokarnik, 1991), aeronautical engineering (Branover and Unger, 1998) etc.

References

Alabort, E., Kontis, P., Barba, D., Dragnevski, K., Reed, R.C., 2016. On the mechanisms of superplasticity in Ti - 6Al - 4V. Acta Mater. 105, 449–463.

Branover, H., Unger, Y., 1998. Progress in Fluid Flow Research: turbulence and Applied MHD. American Institute of Aeronautics and Astronautics, Reston, Virginia.

Buckingham, E., 1914. On physically similar systems; illustrations of the use of dimensional equations. Phys. Rev. 4, 345–376.

Chai, F., Zhang, D., Li, Y., Zhang, W., 2013. High strain rate superplasticity of a fine-grained AZ91 magnesium alloy prepared by submerged friction stir processing. Mater. Sci. Eng. A 568, 40–48.

Dorn, J.E., 1955. Some fundamental experiments on high temperature creep. J. Mech. Phys. Solids 3, 85–116.

El Mehtedi, M., Spigarelli, S., Evangelista, E., Rosen, G., 2009. Creep behaviour of the ZM21 wrought magnesium alloy. Mater. Sci. Eng. A 510–511, 403–406.

Esnault-Pelterie, R., 1950. Dimensional Analysis and Metrology: (the Giorgi System). F. Rouge.

Evans, R.W., Wilshire, B., 1993. Introduction to Creep. Institute of Materials, London.

Frost, H.J., Ashby, M.F., 1982. Deformation-mechanism maps: The plasticity and Creep of Metals and Ceramics. Pergamon, Oxford.

Garofalo, F., 1965. Fundamentals of Creep and Creep-rupture in Metals 91. Macmillan, New York, pp. 49–61 159–201.

Ghosh, A.K., Raj, R., 1981. Grain size distribution effects in superplasticity. Acta Metall. 29, 607–616.

Harper, J., Dorn, J.E., 1957. Viscous creep of aluminum near its melting temperature. Acta Metall. 5, 654–665.

Harry, S., Junghyun, C., 2016. Superplasticity from viscous flow in high Pb ternary alloy. Mater. Sci. Eng. A 658, 210–220.

Imayev, R., Gabdullin, N., Salishchev, G., 1997. Effect of grain size on superplasticity of an intermetallic Ti3Al compound. Intermetallics 5, 229–236.

Kaibyshev, O.A., 1992. Superplasticity in Alloys. Intermetallides and Ceramics.

Kurth, R., 1972. Dimensional Analysis and Group Theory in Astrophysics. Pergamon, New York.

Lavinia, B., Martin, S., Jacques, R., Bernard, V., 2014. Creep behavior of Ti-6Al-4V from 450 °C to 600 °C. U.P.B. Sci. Bull., Series B 76.

Li, X., Lü, X., Wu, H., Ji, B., Chen, J., Li, J., 2017. Effect of grain size on the superplastic deformation behavior of Ti-55 alloy. Procedia Eng. 207, 1880–1885.

Lin, H., Alexander, K.B., Becher, P.F., 1996. Grain size effect on creep deformation of alumina-silicon carbide composites. J. Am. Ceram. Soc. 79, 1530–1536.

Liu, F.C., Ma, Z.Y., 2011. Superplasticity governed by effective grain size and its distribution in fine-grained aluminum alloys. Mater. Sci. Eng. A 530, 548–558.

Lv, X., Wei, J.L., Ji, N.Q., Yi, F.C., Di, Z., Min, M.W., Feng, Z., Bo, J., 2009. Steady state creep of in situ Ti B plus La2O3 reinforced high temperature titanium matrix composite. Mater. Sci. Eng. A 499, 500–506.

Mannan, S.L., Rodriguez, P., 1983. Effect of grain size on creep rate in type 316 stainless steel at 873 and 973 K. Metal Sci. 17, 63.

McKelvey, J.M., 1962. Polymer Processing. Wiley, New York, pp. 31.

Mengjia, L., Qinglin, P., Yunjia, S., Xue, S., Hao, X., 2017. High strain rate superplasticity in an Al–Mg–Sc–Zr alloy processed via simple rolling. Mater. Sci. Eng. A 687, 298–305.

Mikhaylovskaya, A.V., Mosleh, A.O., Kotov, A.D., Kwame, J.S., Pourcelot, T., Golovin, I.S., Portnoy, V.K., 2017. Superplastic deformation behaviour and microstructure evolution of near-α Ti-Al-Mn alloy. Mater. Sci. Eng. A 708, 469–477.

Mukherjee, A.K., Bird, J.E., Dorn, J.E., 1969. Experimental correlations for high temperature creep. Trans. ASM 62, 155–179.

Nag, P.K., 2006. Heat and Mass Transfer: A Practical Approach. McGraw-Hill.

National Standards Body, 1948. British Standard.

Padmanabhan, K.A., 1973. On the nature of the stress function for thermally activated flow. Scr. Metall. 7, 137–144.

Padmanabhan, K.A., 1977. A theory of structural superplasticity. Mater. Sci. Eng. A 29, 1–18.

Padmanabhan, K.A., Davies, G.J., 1980. Superplasticity: Mechanical and Structural aspects, Environmental effects, Fundamentals and Applications. Springer, Berlin.

Padmanabhan, K.A., Leuthold, J., Wilde, G., Bhattacharya, S.S., 2015. On the power law description of low-stress uni-axial steady-state high-homologous-temperature deformation. Mech. Mater. 91, 177–193 [See Also: Ali, A. Arsath Abbas, S. Balasivanandha Prabu, G. Wilde, and K. A. Padmanabhan. “Corrigendum to ”On the power law description of low-stress uni-axial steady-state high-homologous-temperature deformation [Mechanics of Materials 91 (2015) 177–193].

Padmanabhan, K.A., Prabu, S.B., Mulyukov, R.R., Nazarov, A., Imayev, R.M., Chowdhury, S.G., 2018. Superplasticity: Common basis For an Ubiquitous Phenomenon. Springer, Berlin.

Raj, S.V., Langdon, T.G., 1989. Creep behavior of copper at intermediate temperatures - I: mechanical characteristics. Acta Metall 37, 843.

Rayleigh, J.W.S.B., 1877. The Theory of Sound. Macmillan and Company.

Sahithya, K., Sabat, R.K., Bibhanshu, N., Avadhani, G.S., Kumar, S., Satyam, S., 2017. Superplasticity in high temperature magnesium alloy WE43. Mater. Sci. Eng. A 687, 85–92.

Sarebanzadeh, M., Roumina, R., Mahmudi, R., Wu, G.H., Jafari, N.H.R., 2015. Enhancement of superplasticity in a fine-grained Mg–3Gd–1Zn alloy processed by equal-channel angular pressing. Mater. Sci. Eng. A 646, 249–253.

Senkov, O.N., Jonas, J.J., 1996. Effect of strain rate and temperature on the flow stress of β-Phase titanium-hydrogen alloys. Metall. Mater. Trans. A 27A, 1312.

Sherby, O.D., Lytton, J.L., Dorn, J.E., 1957. Activation energies for creep of high-purity aluminum. Acta Metall. 5, 219–227.

Sripathi, S., Padmanabhan, K.A., 2014. On the experimental validation of a mesoscopic grain boundary sliding-controlled flow model for structural superplasticity. J. Mater. Sci. 49, 199–210.

Sun, Q.J., Wang, G.C., 2014. Microstructure and superplasticity of TA15 alloy. Mater. Sci. Eng. A 606, 401–408.

Tang, W.N., Chen, R.S., Han, E.H., 2009. Superplastic behaviors of a Mg–Zn–Y–Zr alloy processed by extrusion and equal channel angular extrusion. J. Alloys Compd. 477, 636–643.

Weili, R., Jianting, G., Gusong, L., Jiansheng, W., 2004. Creep characteristic of NiAl-9Mo eutectic alloy. Mater. Trans. 45, 1731–1737.

White, F.M., 2011. Fluid Mechanics, 7th ed. McGraw-Hill Higher Education, London, New York.

Whittaker, M.T., Wilshire, B., 2010. Creep and creep fracture of 2.25Cr–1.6 W steels (Grade 23). Mater. Sci. Eng. A 527, 4932–4938.

Zlokarnik, M., 1991. Dimensional Analysis and Scale-up in Chemical Engineering. Springer Berlin Heidelberg, Berlin, Heidelberg.